行政院國家科學委員會補助專題研究計畫 ■成果報告 □期中進度報告

金屬奈米粒子毒性及肺部之藥物控放

Toxicity of metal nanoparticles and lung administration of drug nanoparticles

計畫類別：■個別型計畫　□整合型計畫
計畫編號：NSC　97 － 2923 － B － 009 － 001 － MY3
執行期間：　97 年 08 月　01 日至　99 年 07 月 31 日

執行機構及系所：國立交通大學 奈米科技研究所

計畫主持人：黃國華教授
共同主持人：
計畫參與人員：Onischuk A 教授
陳昱勳（博士研究生）

成果報告類型(依經費核定清單規定繳交)：□精簡報告　■完整報告

本計畫除繳交成果報告外，另須繳交以下出國心得報告：
□赴國外出差或研習心得報告
□赴大陸地區出差或研習心得報告
■出席國際學術會議心得報告
□國際合作研究計畫國外研究報告

處理方式：除列管計畫及下列情形者外，得立即公開查詢
■涉及專利或其他智慧財產權，□一年■二年後可公開查詢

中　華　民　國　　年　　月　　日

Abstract

The environmental impact of nanoparticles is evident; however, their toxicity due to their nanosize is rarely discussed. Gold nanoparticles (GNPs) may serve as a promising model to address the size-dependent biological response to nanoparticles because they show good biocompatibility and their size can be controlled with great precision during their chemical synthesis. Naked GNPs ranging from 3 nm to 100 nm were injected intraperitoneally into BALB/C mice at a dose of 8 mg/kg/week. GNPs of 3 nm, 5 nm, 50 nm, and 100 nm did not show harmful effects; however, GNPs ranging from 8 nm to 37 nm induced severe sickness in mice. Mice injected with GNPs in this range showed fatigue, loss of appetite, change of fur color, and weight loss. Starting from day 14, mice in this group exhibited a camel-like back and crooked spine. The majority of mice in these groups died within 21 days. Injection of 5 nm and 3 nm GNPs, however, did not induce sickness or lethality in mice. Pathological examination of the major organs of the mice in the diseased groups indicated an increase of Kupffer cells in the liver, loss of structural integrity in the lungs, and diffusion of white pulp in the spleen. The pathological abnormality was associated with the presence of gold particles at the diseased sites, which was verified by ex vivo Coherent anti-Stoke Raman scattering microscopy. Modifying the surface of the GNPs by incorporating immunogenic peptides ameliorated their toxicity. This reduction in the toxicity is associated with an increase in the ability to induce antibody response. The toxicity of GNPs may be a fundamental determinant of the environmental toxicity of nanoparticles.

To elicit the size-dependent carrier ability of GNPs, a synthetic peptide resembling foot-and-mouth disease virus (FMDV) protein was conjugated to GNPs ranging from 2-50 nm in diameter (2 nm, 5 nm, 8 nm, 12 nm, 17 nm, 37 nm, and 50 nm). An extra cysteine was added to the C-terminus of the FMDV peptide (pFMDV) to ensure maximal conjugation to the GNPs, which have a high affinity for sulfhydryl groups. The resultant pFMDV-GNP conjugates were then injected into BALB/c mice. Immunization with pFMDV-keyhole limpet hemocyanin (pFMDV-KLH) conjugate was also performed as a control. Blood was obtained from the mice after 4, 6, 8, and 10 weeks and antibody titers against both pFMDV and the carriers were measured. For the pFMDV-GNP immunization, specific antibodies against the synthetic peptide were detected in the sera of mice injected with 2-nm, 5-nm, 8-nm, 12-nm, and 17-nm pFMDV-GNP conjugates. Maximal antibody binding was noted for 8- to 17-nm-diameter GNPs. The pFMDV-GNPs induced a three-fold increase in the antibody response, as compared to the response to pFMDV-KLH. However, sera from either immunized mouse group did not exhibit an antibody response to GNP, while the sera from pFMDV-KLH-immunized mice presented high levels of binding activity against KLH. Additionally, the uptake of pFMDV-GNP in the spleen was examined by inductively coupled plasma mass spectroscopy (ICP-MS) and transmission electron microscopy (TEM). The amount of GNP accumulation in the spleen correlated to the magnitude of the immune response induced by pFMDV-GNP. In conclusion, we demonstrated the size-dependent immunogenic properties of pFMDV-GNP conjugates. Furthermore, we established that GNPs ranging from 8 nm to 17 nm in diameter may be ideal for eliciting a focused antibody response against a synthetic pFMDV peptide.

We explored the size-dependent impairment of cognition in mice caused by the injection of GNPs. GNPs 17 nm and 37 nm in diameter were injected intraperitoneally into BALB/c mice at doses ranging from 0.5 to

14.6 mg/kg. ICP-MS was performed on brain tissue collected 1, 14, and 21 days after the injection. A passive-avoidance test was performed on day 21. Monoamine levels were determined on day 21. The microscopic distribution of GNPs in the hippocampus was examined using coherent anti-Stoke Raman scattering (CARS) microscopy and transmission electron microscopy (TEM). The results indicated that 17 nm GNPs passed through the blood-brain barrier more rapidly than 37 nm GNPs. Treatment with 17 nm GNPs decreased the latency time, which was comparable to the effect of scopolamine treatment, while 37 nm GNPs showed no significant effect. Dopamine levels and Serotonin levels in the brain were significantly altered by the injection of 17 nm and 37 nm GNPs. GNPs affected dopaminergic and serotonergic neurons. CARS microscopy indicated that 17 nm GNPs entered the Cornu Ammonis (CA) region of the hippocampus, while 37 nm GNPs were excluded from the CA region. TEM verified the presence of 17 nm GNPs in the cytoplasm of pyramidal cells. Here we show that the ability of GNPs to damage cognition in mice was size-dependent and associated with the ability of the particles to invade the hippocampus. The dosage and duration of the treatment should be taken into account if GNPs are used in the future as vehicles to carry therapeutic agents into the brain.

Key Word: gold nanoparticles, toxicity, vaccine, cognition, drug nanoparticles, mice

摘要

奈米粒子對環境的影響是顯著的,但關於奈米粒子粒徑大小不同所造成的毒性差異卻很少被深入探討。因為奈米金粒子具有良好的生物相容性且其粒徑可以藉由調控化學合成過程而被精確的控制,因此奈米金粒子是一個適合作為探討生物體對於奈米粒子粒徑相依反應的系統。粒徑 3 ~ 100 nm 未經修飾的奈米金每周以 8 mg/kg 的劑量靜脈注射到 BALC/c 小鼠體內。3 nm、5 nm、50 nm、100 nm 奈米金粒子未呈現有害的影響;但粒徑介於 8 nm 到 37 nm 間的奈米金粒子導致老鼠患病現象產生。注射粒徑介於 8 nm 到 37 nm 間奈米金粒子的老鼠出現疲勞、食慾降低、毛色改變、以及體重降低等現象。在注射 14 天後,注射奈米金粒子的老鼠出現駝背及脊椎彎曲的現象,半數以上的老鼠在 21 天內即死亡,但注射 3 nm 和 5 nm 奈米金粒子組別的老鼠卻沒有誘導患病或致死的現象產生。在患病組別老鼠各個重要器官的病理切片中發現:肝組織中 Kupffer 細胞的數量增加、肺組織的結構完整性降低、以及脾臟組織的白質分佈散亂。這些生理不正常的現象和藉由體外 Coherent anti-Stoke Raman scattering microscopy 所分析奈米金粒子存在的疾病部位是相關的。使用免疫性的胜肽鍊修飾奈米金表面改善了其原本的毒性,減少毒性是因為誘導抗體反應的能力增加了。而奈米金粒子造成的毒性可視為奈米粒子對環境造成毒性的基礎認知。

類口蹄疫病毒蛋白的合成胜肽鍊(pFMDV)分別接合到粒徑為 2 nm、5 nm、8 nm、12 nm、17 nm、37 nm 及 50 nm 的奈米金粒子上,用以評估奈米金粒子粒徑相依的攜帶能力。因為奈米金粒子對硫氫基具有相當大的親和性,因此我們在 pFMDV 的羧基側加上一個半胱氨酸以達到接合的最大效率。接下來便將接合好的 pFMDV-奈米金粒子打到 BALB/c 小鼠體內,而控制組則是注射 pFMDV 與 keyhole limpet hemocyanin 接合完成的產物。分別在第 4、6、8、10 周進行小鼠採血並進行 pFMDV 及攜帶者所引起免疫反應抗體效價的測定。在 pFMDV-奈米金粒子接合的免疫試驗中,對合成胜肽鍊具有專一性的抗體可以在接合到 2 nm、5 nm、8 nm、12 nm、17 nm 奈米金粒子組別的老鼠血清中被偵測到,最大的抗體接合效果是 8 nm、17 nm 這兩個粒徑大小的奈米金粒子組別。pFMDV-奈米金粒子接合物所誘導的抗體免疫反應比 pFMDV-keyhole limpet hemocyanin 接合物誘導的結果高了 3 倍以上。然而,以 pFMDV-奈米金粒子免疫小鼠的血清並沒有對奈米金粒子產生抗體反應,但以 pFMDV-keyhole limpet hemocyanin 免疫小鼠組別的血清卻會對 keyhole limpet hemocyanin 產生很強的抗體免疫性。此外,pFMDV-GNP 在脾臟組織中的吸收情形也由感應耦合電漿質譜儀和穿透式電子顯微鏡進行分析,結果奈米金粒子在脾臟累積的情形與 pFMDV-GNP 所誘導的強大免疫反應具有高度相依性。總而言之,我們證明了 pFMDV-GNP 的致免疫性是與奈米金粒子的粒徑相關。我們並建立了粒徑在 8 ~ 17 nm 的奈米金粒子或許具有發展成能產生對 pFMDV 具有專一性抗體攜帶者的潛力。

在我們的研究中藉由注射奈米金粒子到小鼠體內來探討其對小鼠認知行為損傷的粒徑特異性。0.5 ~ 14.6 mg/kg 劑量的 17 nm 和 37 nm 奈米金以靜脈注射的方式打到 BALB/c 小鼠體內。腦組織在注射後 1、14、21 天分別取樣並經感應耦合電漿質譜儀分析。且在第 21 天進行規避試驗的測定並測定 monoamine 的含量。且藉由 coherent anti-Stoke Raman scattering microscopy (CARS)和穿透式電子顯微鏡來定位奈米金粒子在海馬迴的分布位置。結果顯示 17 nm 的奈米金粒子比起 37 nm 的奈米金粒子來的快速穿越血腦屏障,且施用 17 nm 的奈米金粒子組別的小鼠較施用 scopolamine 組別縮短了反應的遲滯時間,但 37 nm 的奈米金粒子卻沒有造成顯著差異。並且,腦中的 dopamine 和 serotonin 濃度在注射 17 nm 及 37 nm 奈米金粒子後都有顯著的改變產生,奈米金粒子影響了跟 dopamine 和 serotonin 相關的神經細胞。

CARS microscopy 的實驗結果顯示 17 nm 的奈米金粒子進到海馬迴的 Cornu Ammonis (CA) region，但 37 nm 的奈米金卻被排除在外;且穿透式電子顯微鏡的影像呈現 17 nm 奈米金粒子存在於 pyramidal cell 的細胞質內。在此我們證明了奈米金粒子造成小鼠認知行為損傷的影響是具有粒徑特異性的，且和粒子侵入海馬迴的能力具有相關性。因此，若未來奈米金粒子發展做為攜帶藥物進入腦的載體時，施用的劑量以及施用期間的長短必須要被準確的控制。

關鍵詞: 肺、金屬奈米粒子、毒性、奈米粒子藥物控放

Contents

Introduction

The environmental impact of nanoparticles is evident; however their nanotoxicity due to the reduction in size to nanoscale is rarely discussed. Gold nanoparticles (GNPs) may serve as a promising model to address this size-dependent toxicity, since gold is extraordinarily biocompatible.

Recently, the increased toxicity of nanoparticles due to their tiny physical dimensions has been widely recognized[1-3]. Carbon black is nontoxic; however carbon nanotubes and fullerene are highly toxic when inhaled into the lungs[4-6]. Similarly, enhanced toxicity of titanium oxide nanoparticles has been reported[7-8] and titanium oxide nanoparticles have been shown to induce oxidative stress in bacteria[9]. A large number of non-toxic bulk materials become poisonous when their size is reduced to nanoscale. However, the toxicity may be due more to the unique surface chemistry of the individual nanoparticle and less to the reduction in size per se.

The toxicity of GNPs has been investigated at the cellular level. GNPs enter cells in a size- and shape-dependent manner[10-11]. Uptake of GNPs reaches a maximum when the size nears 50 nm and when the aspect ratio approaches unity. The transport efficiency reaches a plateau 30 min after incubation. The uptake of GNPs is consistent with receptor-mediated endocytosis. Nevertheless, most GNPs can enter cells efficiently, and most studies indicate that they are nearly harmless to cultured cells[12-15].

We have demonstrated that at heavy dose GNPs are lethal to mice. The lethality of GNPs is size-dependent and also is associated with the immunogenicity of GNPs. We demonstrated that GNPs serve as vaccine carriers stimulating enhanced and focused immune response against peptides cross-linked on GNPs. The ability of GNP-peptide conjugate to stimulate immune response is size-dependent. We also demonstrated that GNPs are capable of passing through blood brain barrier, entering mouse brain, invading hippocampus, and impairing the cognition of mice. The dopaminergic and serotonergic neurons are affected in the presence of GNPs.

Materials and Methods

Chemicals

$HAuCl_4$, sodium citrate, $NaBH_4$, HCl, HNO_3, H_2SO_4, H_2O_2, OsO_4, and other analytical grade chemicals were purchased from Sigma-Aldrich and Fisher Scientific. H_2O was obtained at >18 M_ from a Milli-Q water purification system.

Preparation and characterization of GNPs

GNPs with diameters of 2, 5, 8, 12, 17, 37, and 50 nm were synthesized as reported previously[16-17]. The seed colloids were prepared by adding 1 ml of 0.25 mM $HAuCl_4$ to 90 ml of water and stirring for 1 min at 25 ◦C. Two milliliters of 38.8 mM sodium citrate were then added to the solution, followed by stirring for 1 min and the addition of 0.6 ml of freshly prepared 0.1 M $NaBH_4$ in 38.8 mM sodium citrate. The solution was stirred for an additional 5–10 min at 0–4 ◦C. Different GNP diameters, ranging from 2 to 50 nm, were generated by changing the volume of the seed colloid added. Reaction temperatures and times were adjusted to obtain GNPs of a larger size. All synthesized GNPs were characterized by ultraviolet (UV) light absorbance and their size was verified by electron microscopy and atomic force microscopy. The potential difference between the dispersion medium and the stationary layer of fluid attached to the dispersed GNPs was characterized by zeta potentials (table 1). Zeta potentials of both GNPs fell between ±40 and 60 mV, indicating good stability of the colloidal gold in the solution. To minimize the impact of unreacted chemicals on the experimental animals, the GNPs were further purified by precipitation at 10000 rpm in a microcentrifuge, followed by dialysis against phosphate-buffered saline (PBS; pH 7.4) before injection into the animals.

Table 1. Size distribution and zeta potentials of 17 nm (sample A) and 37 nm (sample B) GNPs. The size distribution and zeta potential of the gold nanoparticles was determined by a Delsa Nano C (NCTU Instruments Ltd, Hsinchu, Taiwan). The GNPs were resuspended in phosphate buffer (pH 7.4, 0.1 M) and the zeta potentials were measured at 25 ◦C.

Sample	Particle size (nm)	Zeta potential (mV)
A	17 ± 1.5	−45.9
B	37 ± 2.1	−47.8

Lethality Test

Mice were randomly assigned to experimental groups. Each group consisted of 6 mice. Administration of GNPs was performed by intraperitoneal injection. Animals were sacrificed at the end of experiment by cervical dislocation. The liver, lung, brain, heart, and spleen were isolated, and organ weights of all mice were measured.

Passive-avoidance test [18]

The apparatus consisted of two compartments with a steelrod grid floor (supporting information, figure 2S (available at stacks.iop.org/Nano/21/485102/mmedia); 36 parallel steel rods, 0.3 cm in diameter, set 1.5 cm apart). One of the compartments (48 cm × 20 cm × 30 cm) was equipped with a 20 W lamp located in the center of the apparatus at a height of 30 cm and the other was a dark compartment of the same size. The compartments were connected through a guillotine door (5 cm × 5 cm). The dark room was used during the experimental sessions that were conducted between 09:00 and 17:00 h. During the training trial, the guillotine door between the light and dark compartments was closed. When the mouse was placed in the light compartment with its back to the guillotine door, the door was opened and the time until the mouse entered the dark compartment (step-through latency, STL) was measured with a stopwatch. After the mouse entered the dark compartment, the door was closed. A 1 mA scrambled footshock was delivered through the grid floor for 2 s. The mouse was removed from the dark compartment 5 s after the shock. Then, the mouse was put back into the home cage until the retention trial was carried out 24 h later. The mouse was again placed in the light compartment and, similar to the training trial, the guillotine door was opened and the step-through latency was recorded. If the mouse did not step through the door after 300 s, the experiment was ended.

Analysis of monoamine and acetylcholine concentrations in the mouse brain

Monoamine levels were determined as previously reported[18]. The mice were decapitated and their brains were quickly removed. The brain samples were weighed and homogenized on ice using a Polytron homogenizer (Kinematica, Lucerne, Switzerland) at the maximum setting for 20 s in 10 volume equivalents of 0.2 M perchloric acid containing 100mMNa_2-EDTA and 100 ng ml^{-1} isoproterenol. The homogenate was centrifuged at 15 000*g* for 30 min. The pH was adjusted to approximately 3.0 using 1 M sodium acetate. After filtration (0.45 μm), the samples were separated using high performance liquid chromatography (HPLC). Monoamines and their metabolites were separated using HPLC at 30 ◦C on a reverse-phase analytical column (ODS-80, 4.6 mm i.d. × 15 cm) and detected by an electrochemical detector (Model ECD-100, Eikom Co., Kyoto, Japan). The column was eluted with 0.1 M sodium acetate–citric acid buffer (pH 3.5) containing 15% methanol, 200 mg l^{-1} sodium 1-octanesulfonate and 5 mg l^{-1} Na_2-EDTA. The following monoamines and their metabolites were measured: norepinephrine (NE), 4-hydroxy-3-methoxyphenylglycol (MHPG), dopamine (DA), 3,4-dihydroxyphenylacetic acid (DOPAC), 5- hydroxytyramine (5-HT, serotonin) and 5-hydroxyindoleacetic acid (5-HIAA).

Acetylcholine (Ach) levels were determined as previously described[18]. The HPLC system (DSA-300, Eicom) consisted of a detector with a platinum electrode. A guard column and an enzyme column were placed before and after the analytical column (4.6mm×160 mm, Eicompak AC-GEL; Eicom), respectively. Isopropylhomocholine was added to the sampling tubes as an internal standard, and the mixture was analyzed using HPLC. The mobile phase was 0.1 M phosphate buffer (pH 8.3), and the flow rate was 0.6ml min−1. Ach levels in the sample were quantified by using the internal standard method.

Design of synthetic peptide

The sequence of pFMDV is (N-terminus) NGSSKYGDTSTNNVRGDLQVLAQKAERTL (C-terminus), representing amino-acid residues 131–159 of the VP1 protein of the FMDVO/Taiwan/97strain. The peptide sequence was synthesized with an added C-terminal cysteine residue using an ABI Peptide Synthesizer and Fmoc chemistry. The sequence of the generated peptide was then verified by mass spectrometry and amino-acid composition analysis.

Preparation of pFMDV–carrier conjugates

KLH conjugates were synthesized as reported previously[19]. The cysteine-containing pFMDV was resuspended in distilled water at 1 mg ml^{-1} and the pH was adjusted to approximately 8.5 by the addition of dilute sodium hydroxide. Commercial maleimide-activated KLH (Pierce, Rockford, IL, USA) was reconstituted in 50 mM sodium phosphate, 0.15 M NaCl, and 0.1 M EDTA buffer (pH 7.2) at a final concentration of 10 mg ml^{-1}. The peptide and carrier were mixed at a 0.5 molar ratio of thiol to maleimide in 0.1 M sodium phosphate, 0.15 M NaCl, and 10 mM EDTA buffer (pH 7.2) and allowed to react at 25 ◦C, shielded from light. The conjugated complexes were purified by centrifugation and resuspended in PBS to a final concentration of 0.01 mg ml^{-1}. The conjugate was then separated from unreacted peptide and carrier by high performance liquid chromatography (HPLC).

The approach used to conjugate GNPs to peptide was based on titration methods[20]. An extra cysteine was added to the C-terminus of each peptide to improve binding to the surface of the GNPs. GNP–peptide conjugation was achieved by titrating the antigens into a GNP solution. This titration was monitored by UV absorption at the wavelength appropriate for each peptide to detect aggregation of unsaturated GNPs in the presence of 1 M NaCl. After reaching the saturation point, the conjugated complexes were purified by centrifugation and resuspended in PBS to a final concentration of 0.01 $\mu g\ \mu l^{-1}$.

Immunization of mice

Animal treatments were performed following the 'Guidelines for the Care and Use of Experimental Animals' issued by National Chiao Tung University (Hsinchu, Taiwan). Fourweek- old male BALB/c mice were housed at 22 ± 2 ◦C in a 12 h light/dark cycle and fed standard rodent chow and water *ad libitum*. Mice were randomly assigned to experimental groups, with each group consisting of six mice.

Groups of 4-week-old BALB/c mice were administered intraperitoneal (IP) and subcutaneous (SC) immunizations containing (1) pFMDV–KLH conjugate or (2) pFMDV–GNP conjugates with diameters of 2, 5, 8, 12, 17, 37, or 50 nm. These antigens were administered in equal volumes of complete Freund's adjuvant. For all groups, the mice were immunized at weeks 0, 1, 2, 3, 5, 7, and 9 and blood was collected from the tail vein after 4, 6, 8, and 10 weeks. The sera were collected after centrifugation and stored at −20 ◦C. Animals were sacrificed at the end of the experiment by cardiac puncture under carbon dioxide anesthesia. The spleens were then isolated and the organ weights of all mice were measured.

Enzyme-linked immunosorbent assay (ELISA)

To coat a 96-well plate with GNP, each well was pretreated with 200 μl of 1 mM 3-aminopropyl-triethoxysilane (APTES) in ethanol at room temperature for 40 min. APTES encourages optimal crosslinking of GNPs to plastic wells, allowing an effective ELISA to be conducted[21]. The activated wells were washed with ethanol twice for 5 min, followed by distilled water for 5 min. GNPs (15 mM, 150 μl) were then added to the coated wells and incubated for 2 h at room temperature, followed by three distilled water washes and three washes with 0.5% Triton X-100 in PBS. To coat the wells with other antigens, 100 μl of antigen were added to the wells, followed by incubation at room temperature for 30 min and three PBS washes. Blocking of non-specific binding was performed by adding 100 μl of 3% BSA to the wells for 60 min at room temperature, followed by three PBS washes. Antibody binding was then conducted by adding 100 μl of diluted antiserum to the wells and incubating for 1 h at room temperature, followed by further washes with PBS. To develop the ELISA, horseradish peroxidase (HRP) conjugated anti-mouse immunoglobulin G (IgG), 2,2_-azinodi-(3 ethylbenzthiazoline sulfonic acid) (ABTS), and hydrogen peroxide were added to the wells sequentially, according to the manufacturer's instructions, and the antibody–antigen binding efficacy was monitored by measuring absorbance at 405 nm.

Gel electrophoresis

Samples were mixed with 1% Tris-buffered saline (TBS; Sigma-Aldrich) and loaded onto a 3% agarose gel (Sigma- Aldrich). Gel separation was then performed using an electrophoresis unit running at 80 V. Protein levels were then visualized by incubating the gels in Coomassie Brilliant Blue R-250 staining solution (Sigma-Aldrich), followed by washing in a destaining solution containing 70% methanol and 7% acetic acid.

Inductively coupled plasma mass spectrometry (ICP-MS)

For the total element determinations, standard solutions were prepared by diluting a multi-element standard (1000 mg l^{-1} in 1 M HNO_3) obtained from Merck (Darmstadt, Germany). Nitric acid (65%), hydrochloric acid (37%), perchloric acid (70%), and hydrogen peroxide (30%) of Suprapur® grade (Merck) were used to mineralize the spleen sections. These samples were then homogenized in 25 mM Tris and 12.5 mM HCl solution (pH 8) and centrifuged at 13 000 rpm for 1 h. The resultant supernatant was applied to the size-exclusion column of the HPLC system, which had been equilibrated with 25 mM Tris and 12.5 mMHCl buffer (containing 20 mM KCl), and eluted with the same buffer at a flow rate of 1 ml min^{-1}. The eluted fractions from the HPLC system were detected by ICP-MS (SCIEX ELAN 5000, Perkin Elmer) and the metal components were identified using a gold standard. The main operating conditions were as follows: RF power of 1900 W, carrier gas flow of 0.8 lmin−1 Ar, and makeup gas flow of 0.19 l min^{-1} Ar. The isotope 197Au was measured as an internal standard.

Ex vivo coherent anti-Stokes Raman scattering (CARS) microscopy

Freshly removed hippocampi were dissected into thin slices, approximately 2 mm in thickness, and immersed in a microchamber on a glass slide under PBS for examination. CARS microscopy was performed with a time constant of 3 ms, a scanning area of 300 μm × 300 μm, a step size of 1 μm, 300 pixels × 300

pixels, a scanning velocity of 1 μmms^{-1} and a sampling rate of 80 kHz. The laser power was set at 30 mW for 870 nm and 40 mW for 1064 nm. The wavelengths of the pump and the Stokes lasers (Pump = 870 nm and Stokes = 1064 nm) were tuned to match a Raman shift (~2100 cm^{-1}) that falls in the so-called 'silent region' of the vibrational spectra of cells and tissues. As expected, the CARS images of the 'control' did not show appreciable contrast under the non-resonant condition, whereas the CARS signals were dramatically enhanced, i.e. they appeared as scattered bright spots on the images taken from the GNP-treated specimens. The enhancement presumably resulted from strong scattering by the GNPs and the large thirdorder polarizability of the GNPs[22-25].

Transmission electron microscopy (TEM)

Small pieces of tissue were fixed in 2.5% glutaraldehyde in 0.05 M sodium cacodylate-buffered saline (pH 7.4) at room temperature for 2 h. This primary fixation was followed by three 20 min washes with 0.05 M sodium cacodylate-buffered saline. The samples were then placed into 1% OsO_4 in sodium cacodylate-buffered saline at room temperature for 1 h. OsO_4 fixation was followed by three 20 min distilled water washes and dehydration in acetone. The samples were transferred successively to 33% and 66% Spurr resin/acetone solutions for 30 min each, followed by 100% Spurr resin for 5 h and fresh resin overnight.

Ultrathin 100 nm sections were produced using an ultramicrotome. The grids with ultrathin sections were poststained with uranyl acetate for 30 min followed by lead for 3 min. After the post-staining procedure, a thin layer of carbon was evaporated onto the surface of the grids. The ultrathin sections were then examined using a Jeol 1400 and 3200 FS TEMs.

Statistical analyses

All data are presented as the mean ± SEM, with a minimum of six mice in each group. Concentrations of biogenic amines and Au in the spleen were analyzed using the unpaired Student's *t*-test. The criterion for statistical significance was $p < 0.05$ for all analyses.

Results and Discussions

GNPs Ranging from 8 to 37 nm Induced Severe Sickness in Mice

GNPs were synthesized with diameters ranging from 3 to 100 nm according to published procedures [16-17]. Synthesis of GNPs was monitored by UV absorbance, and the size was examined by electron microscopy (Fig. 1). The purified GNPs had diameters of 3, 5, 8, 17, 12, 37, 50, and 100 nm. They were injected intraperitoneally into BALB/C mice at a dose of 8 mg/kg/week. Mice injected with 3, 5, 50, and 100 nm GNPs behaved normally and survived throughout the experimental period. Mice injected with 8, 17, 12, and 37 nm GNPs exhibited symptoms of toxicity. The treated animals showed fatigue, loss of appetite, change in fur color, and weight loss. There was a dramatic difference in the fur color of GNP-treated mice compared to the normal group, which was usually brownish. The skin underneath had minor rashes, bruising, and hemorrhaging. Starting from day 14, mice injected with 8–37 nm GNPs showed a significantly camel-like back and crooked spine. The majority of mice in these groups died before the end of the fourth week. The median survival time, defined as the length of time when half the mice died, was approximately 21 days for mice injected with 8–37 nm GNPs (Fig. 2).

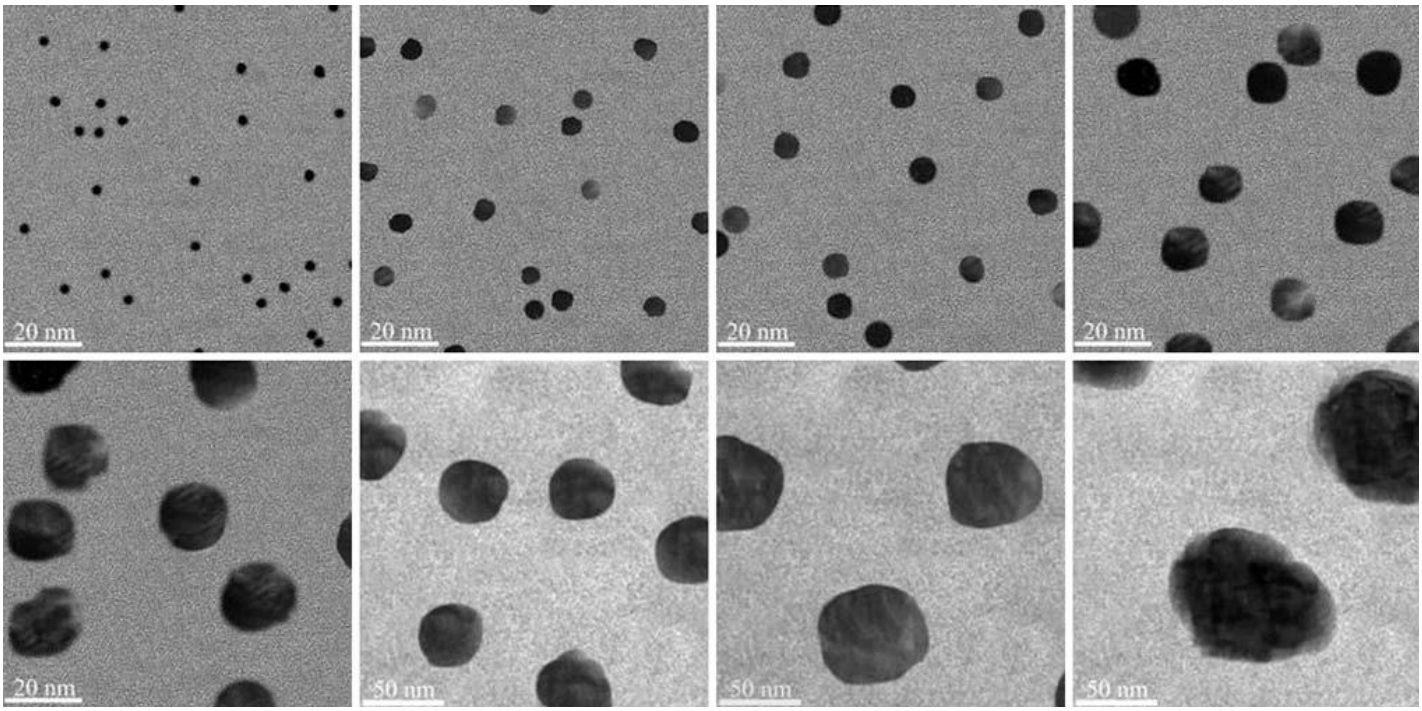

Fig. 1 TEM images for the GNPs synthesized in the current study. GNPs with diameters of 3, 5, 8, 12, 17, 37, 50, and 100 nm were examined under an electron microscope. Scale bars are 20 nm for images of 3, 5, 8, 12, and 17 nm GNPs. Scale bars are 50 nm for images of 37, 50, and 100 nm GNPs

Pathological Abnormalities in GNP-Treated Mice Correlated with the Presence of GNPs in Organs

The acute symptoms and eventual death of mice receiving GNPs indicated that the injected GNPs might damage major organs. In the tissues samples stained with haematoxylin and eosin, the brain, heart, and kidney from 8 to 37 nm GNP-treated mice appeared indistinguishable from tissues in control mice (data not shown). However, the liver, lung, and spleen from 8 to 37 nm GNP-treated mice showed various degrees of abnormality (Fig. 3).

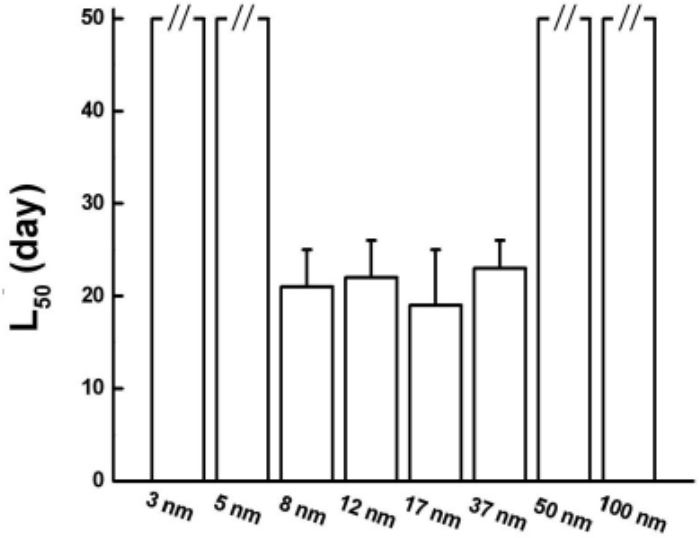

Fig. 2 Average lifespan of mice receiving GNPs with diameters between 8 and 37 nm was shortened to different extents. The average lifespan (L50) was defined as the time beyond which half of the mice died. Mice injected with GNPs outside the lethal range behaved normally. The break marks on the top of bars indicate no death observed during the experimental period

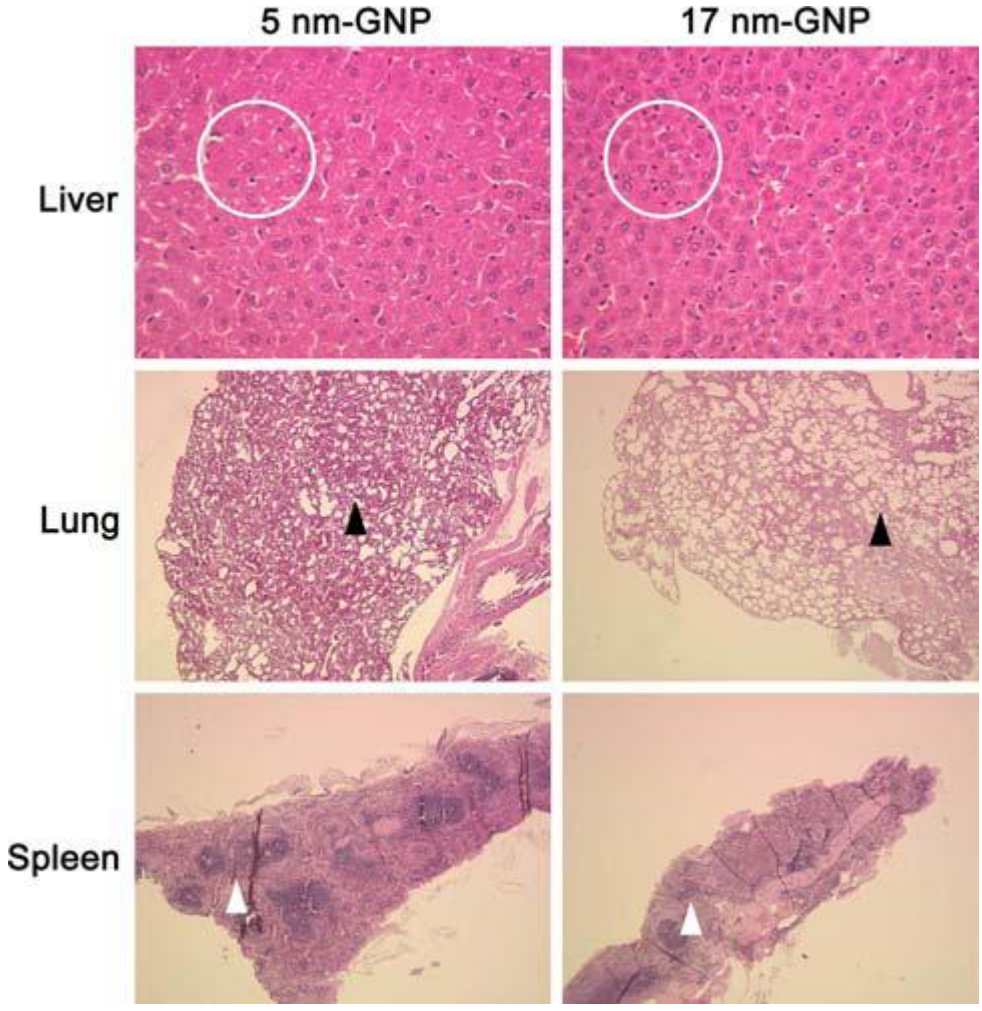

Fig. 3 H&E staining showed GNP-induced abnormality in major organs. (Top to bottom) HE staining for liver, lung, and spleen. The left column shows tissues from 5 nm GNP-treated animals. The right column shows tissues from 17 nm GNP-treated mice

For example, an increase of Kupffer cells (KCs) in the liver was observed in GNP-treated mice. KCs constitute the first macrophage population of the host to come in contact with bacteria, endotoxins, and microbial debris derived from the gastrointestinal tract and transported to the liver. KCs are an important component of the initial and rapid response to potentially dangerous stimuli. Activation of KCs suggested toxic potential for GNPs in this zone[26]. Quantitatively, significant increase of KCs in the liver of 12, 17, and 37 nm GNP-treated mice was observed. Among them, two-fold increase of KCs was observed in 37-nm treated group. GNPs smaller than 8 nm (3 and 5 nm) or larger than 37 nm (50 and 100 nm) did not induce significant KC variations in mouse livers.

Damage in lung tissue structure observed in GNP-treated mice appeared to be similar to that of emphysema. In emphysema, the tiny air sacs (alveoli) in the lungs through which oxygen is absorbed into the bloodstream lose their natural elasticity. Emphysema is a progressive lung condition that leaves sufferers struggling for breath, leading to fatigue, weight loss, and eventually death. Emphysema- like structure was observed in the lung of 8, 12, 17, and 37 nm GNP-treated mice. Other groups did not show aberrant lung structure.

Significant aberration of white pulp was observed in the spleen from GNP-treated mice. The white pulp normally consists of aggregates of lymphoid tissue and is responsible for the immunological function of the spleen. White pulp consisting of splenic nodules appeared diffused in the experimental group. Diffused white pulps were observed in the spleen of 8, 12, 17, and 37 nm GNP-treated mice. Other groups did not show this aberration.

Contaminants of the GNP preparations, such as endotoxins, may have caused damage to organs leading to death. However, all GNPs went through the same synthesis and purification procedure, but GNPs outside the lethal range exhibited no toxic effects on mice. Furthermore, the ELISA using anti-Gram negative endotoxin-IgG showed negative results against all GNPs (Fig. 4). We can therefore exclude the possibility of endotoxin contamination as an explanation for the toxic effects observed in the GNPtreated mice.

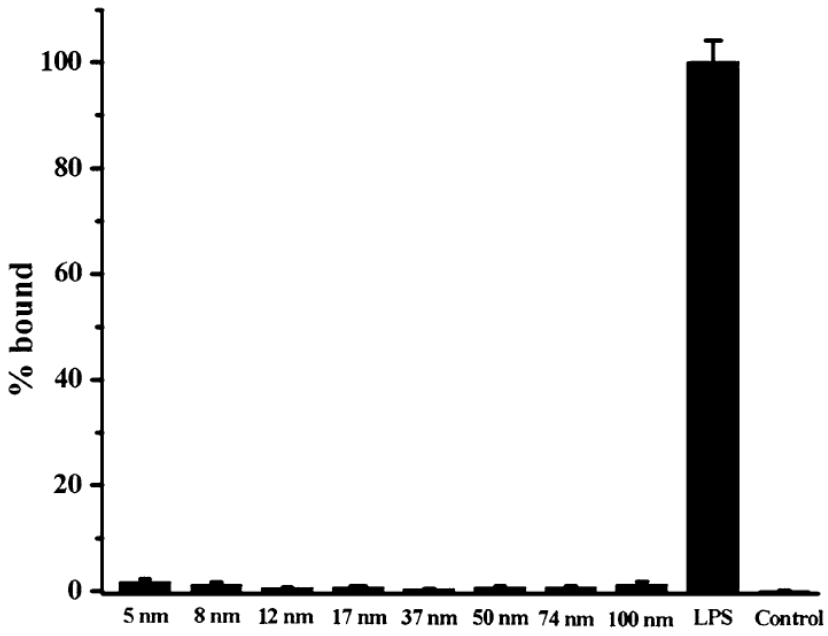

Fig. 4 ELISA of GNPs using anti-endotoxin IgG. ELISA was performed by using anti-endotoxin IgG against various sizes of GNPs synthesized in the lab. Lipopolysaccharide (LPS) served as a positive control, while BSA served as a negative control

It is possible that the abnormalities in the liver, lung, and spleen of GNP-treated mice may have been the consequence of direct contact with the invading GNPs. The injected GNPs may have been transported through blood veins or through diffusion into the liver, lung, and spleen.

To verify the presence of GNPs at the site of abnormality, ex vivo CARS microscopy was performed on the freshly dissected liver tissues[27] (Fig. 5). GNPs are known to enhance the anti-Stoke Raman signal of nearby amino acids. By applying proper controls, CARS microscopy can detect GNPs by measuring this enhancement. Ex vivo diffusion of GNPs into liver tissues was also performed to verify the enhancement of the Raman signal. Localized enhancement of the anti-Stroke Raman signal at an excitation wavelength of 817 nm was observed for livers removed from 8 to 37 nm GNP-treated mice. A significantly weaker signal was observed with livers from 50 nm GNP-treated mice. The Raman signal was totally absent for tissues from 5 nm GNP-treated mice, and tissues from the control group showed no enhancement. The intensity of the Raman signal in the CARS microscopy was proportional to the severity of illness. Our evidence indicates that the dysfunction of major organs is associated with the presence of GNPs at the site of abnormality. Inductively coupled plasma mass spectrometry (ICP-MS) is capable of determining the biodistribution of GNPs with different sizes. Detailed biodistribution profiles could give more useful information to explain the mechanism of toxicity[28-29]. Future experiments will be performed regarding this method.

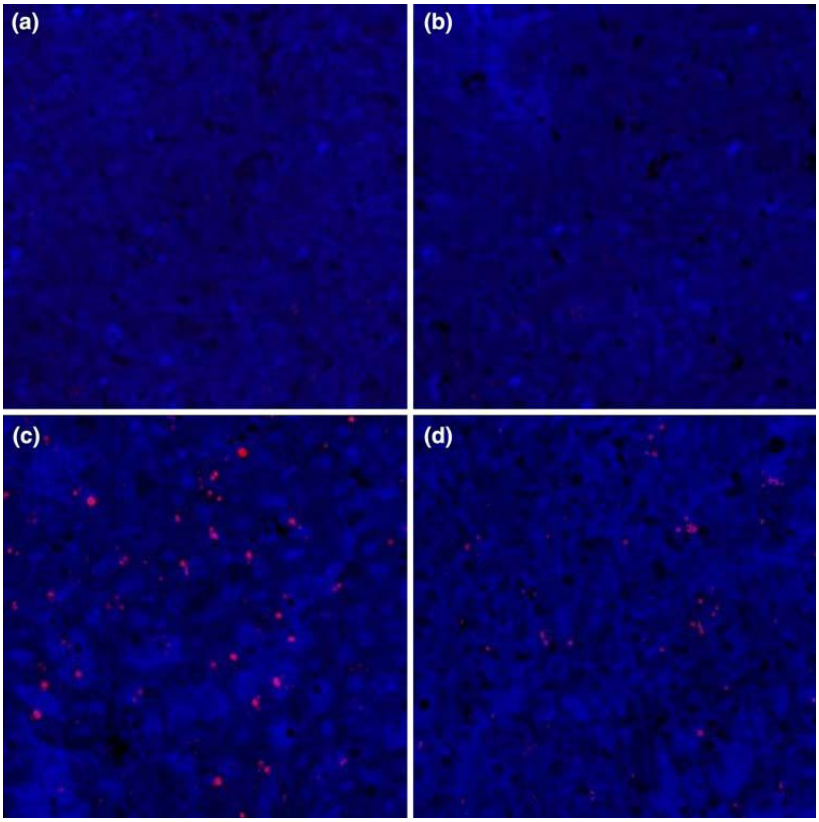

Fig. 5 CARS microscopy of livers isolated from GNPtreated and control mice. The wavelengths of the pump and the Stokes lasers (Pump = 870 nm and Stokes = 1064 nm) were tuned to match a Raman shift (*2100 cm^{-1}), falling in the so-called ‘‘silent region’’ of the vibrational spectra of cells and tissues. As expected, the CARS images of the ‘‘control’’ did not show appreciable contrast under the non-resonant condition whereas the CARS signals were dramatically enhanced and appeared as scattered bright spots on the images taken from the specimens treated with GNPs. The enhancement presumably resulted from strong scattering from the GNPs and the large third-order polarizability of the GNPs. Enhanced bright spots were observed in neither the control group (a) nor the mice injected with 5 nm GNP (b). Livers obtained from 17 nm GNPtreated mice showed intense bright spots (c). Livers obtained from 50 nm GNP-treated mice showed only a moderate number of spots (d)

Enhanced Immunogenicity Ameliorated the Harmful Effect of GNPs

Study of GNP transport using Hela cells indicated that the maximal endocytosis of GNPs occurs when the particles have a diameter of 50 nm[2]. In the current study, injection of 50 nm or larger GNPs, however, did not lead to the death of mice, consistent with the observation that the cell membrane prevents the passage of particles larger than 200 nm. In vivo aggregation of GNPs may have occurred to increase the apparent particle size and lead to the retardation of cellular uptake[30]. We observed that GNPs smaller than 37 nm were lethal to mice, while a further reduction to 5 nm was nontoxic. The alleviation of the lethal effect for 3 and 5 nm GNPs remains to be explored.

It is possible that the difference in lethality may reflect a difference in cellular toxicity. A colorimetric methyl-thiazol- tetrazolium (MTT) assay was performed to measure the cytotoxicity of GNPs in cultured Hela cells. The viability of cells exceeded 80% at the highest concentration of GNP (0.4 mM), indicating that regardless of their size, all GNPs were essentially non-toxic to Hela cells (Fig. 6). The inconsistency of cytotoxicity and lethality indicated that factors other than cytotoxicity may be involved in the amelioration of the lethal effect for 3 and 5 nm GNPs.

We have previously shown that serum obtained from mice injecting with 5 nm GNPs showed specific binding activity to GNPs, while serum from mice immunized with larger-sized GNPs showed only background binding[31]. This differential immune response of mice to different sizes of GNPs indicates that the scavenging activity of the immune system may play a role in the size-dependent lethality of GNPs. To test this hypothesis, surface modification of 17 nm GNPs was carried out so that they would display a spectrum of epitopes. The highly immunogenic peptides pFMDV and pH5N1 were designed and synthesized based on viral protein 1 of foot-and-mouth disease virus type O and matrix protein 2 of influenza A virus (A/Hong Kong/482/97(H5N1)), respectively. BSA and lysozyme were selected to represent moderately immunogenic antigens. As a positive control, mice were injected with unmodified 17 nm GNPs. Injection of surface-modified GNPs caused a spectrum of lethality in mice (Fig. 7). pFMDV and pH5N1 conjugation extended the average lifespan from 21 days to more than 50 days. Lysozyme modification elongated the lifespan to 27.5 days, while BSA modification caused elongation to 22.3 days. The titer of antigen binding activity of sera was verified by ELISA (Fig. 7). Sera obtained from groups injected with pFMDV and pH5N1-conjugated 17 nm GNPs exhibited the highest titer. Lysozyme- and BSA-coated GNPs induced moderate titers. The ability of coated-GNPs to reduce the lethal effect was closely associated with their ability to induce an antibody response. In rodents, quantum dots with final hydrodynamic diameter \5.5 nm resulted in rapid and efficient urinary excretion and elimination from the body[32]. Urinary secretion may play an important role to remove GNPs under 5 nm in our model.

GNPs caused a range of lethality when injected into mice. GNPs larger than 50 nm were nontoxic to mice, which can be interpreted as a diffusion-restricted region. The nontoxic effect of GNPs smaller than 5 nm can be explained by the increase in antibody response that enhanced the scavenging effect. Apparently, the lethal effect is due to the inability of GNPs to stimulate a strong immune response, which allows them to diffuse freely into cells.

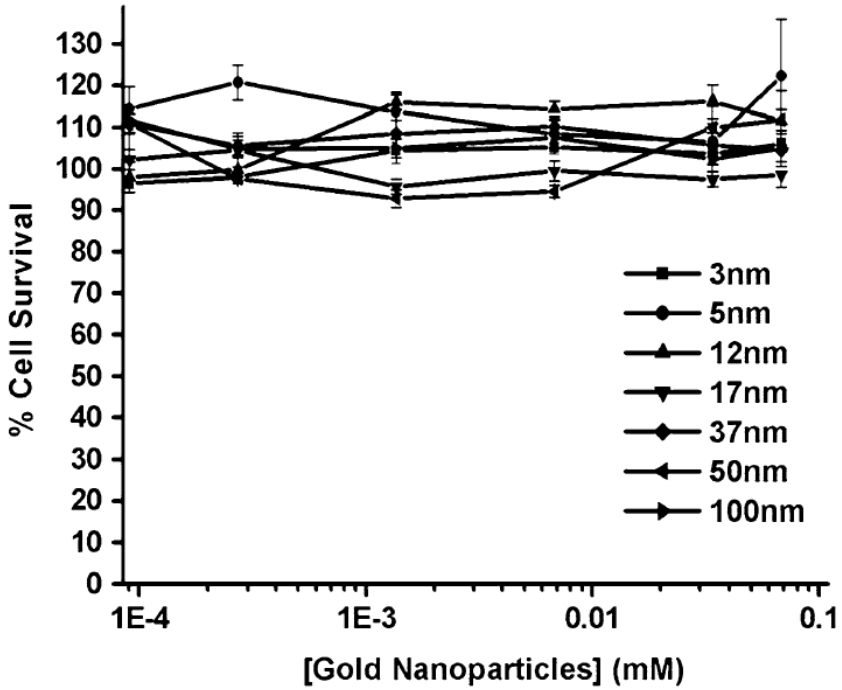

Fig. 6 MTT assay to obtain LC50 for different sizes of GNPs using Hela cells as a model system. After seeding and proper attachment, the Hela cells were treated with 5, 8, 12, and 17 nm GNPs at the concentrations, indicated on the horizontal axis. The percentage of survival was plotted against GNPs concentration

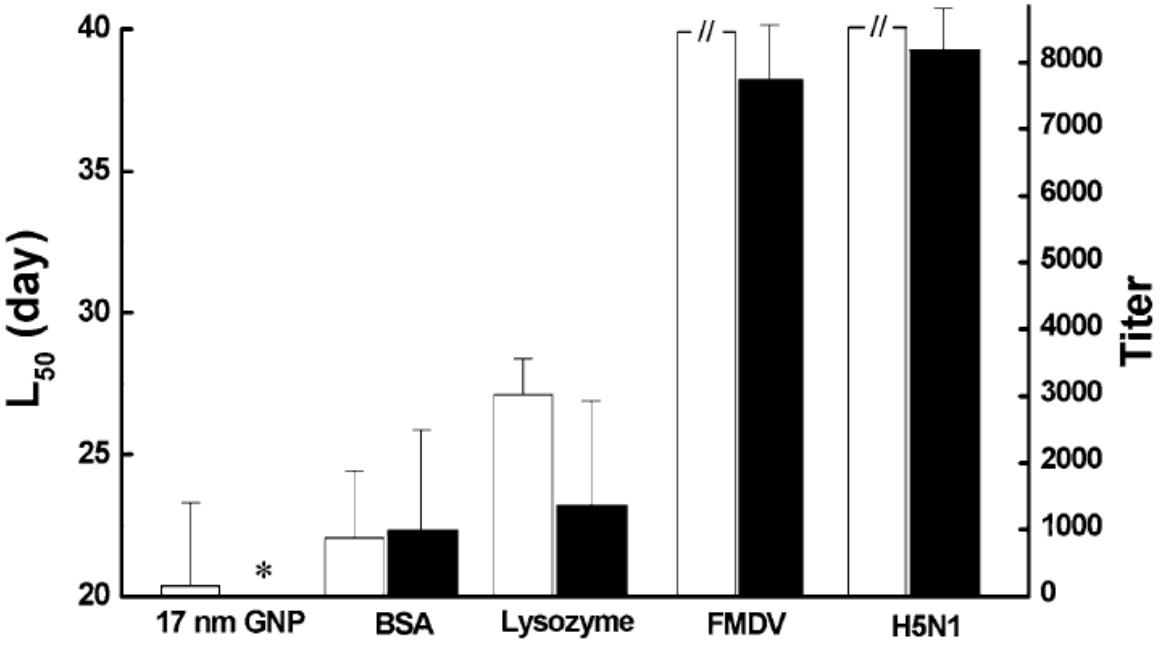

Fig. 7 The lethality and immunogenicity of surface-modified 17 nm GNPs. Average lifespans of mice injected with modified 17 nm GNPs are shown in empty columns. Each experimental group received GNP conjugated with BSA, lysozyme, pFMDV, or pH5N1. Unmodified GNPs served as a positive control (17 nm GNP). Titers of antiserum withdrawn from GNP-injected mice against corresponding antigens are shown in filled columns. pH5N1- and pFMDV-coated GNPs induced the highest titer in mouse serum; BSA- and lysozyme-coated GNPs induced a moderate titer; and unmodified GNPs did not induce an antibody response in mice (*)

Dose-dependent biodistribution of GNPs in mouse brain

GNPs (17 and 37 nm in diameter) were synthesized according to published procedures[16-17]. The synthesis was monitored by UV absorbance, and the particle size was examined by electron microscopy (17 ± 1.5 nm and 37 ± 2.1 nm). The potential difference between the dispersion medium and the stationary layer of fluid attached to the dispersed GNPs was characterized by zeta potentials (table 1). Zeta potentials of both GNPs fell between ±40 and 60 mV, indicating good stability of the colloidal gold in the solution. The purified GNPs were injected intraperitoneally into the BALB/c mice at doses of 0.5–14.6 mg kg^{-1}. ICP-MS was performed on brains sampled at 1, 14 and 21 days after the injection to evaluate residual GNPs in the brain (figure 8). GNPs were detected in brain samples one day after the injection. GNPs accumulated rapidly in the first two weeks and continued to increase until the end of the third week. For all dosages, the amount of 17 nm GNPs deposited in the brain was approximately 20% higher than the amount deposited for 37 nm GNPs on days 1 and 14, while the levels were similar on day 21. It is likely that the 17 nm GNPs passed through the blood–brain barrier more readily than 37 nm GNPs, resulting in faster initial accumulation. However, the GNP levels were comparable on day 21. When the dosage of either GNP was higher than 7.3 mg kg^{-1}, symptoms of toxicity were noted in the mice at day 21. The treated animals showed fatigue, loss of appetite, changes in fur color and weight loss. Starting from day 21, the mice showed a significantly camel-like back and a crooked spine. These symptoms were consistent with previous results showing that high doses of GNPs induced multiple abnormalities in mice[25].

GNPs impair learning and memory in mice

To explore if the injected GNPs retarded brain function in mice, particularly learning and memory, we examined the passive avoidance performance of GNP-treated mice at a GNP dose of 3.7 mg kg^{-1}. The dose was chosen as a minimal dose to avoid the lethal effect of GNPs. Previously, we demonstrated that the lethal dose of GNPs was 8 mg/kg/week for four consecutive weeks. However, the current study employed lower doses, which only caused minor symptoms in mice. Scopolamine has the potential to induce amnesia and was applied as the positive control (figure 9(A)). Untreated mice exhibited a latency of 180 ± 9 s. Scopolamine induced amnesia, resulting in an avoidance latency of 92 ± 22 s, a 50% reduction compared to the untreated controls ($p < 0.01$). Although both GNPs caused weakness in mice, an insignificant reduction in latency was observed for the 37 nm GNP-treated mice, while the 17 nm GNP-treated mice showed a latency of 81 ± 25 s in the passive-avoidance performance test ($p < 0.01$). The latency in the 17 nm GNP-treated mice was comparable to the amnesia caused by scopolamine treatment. Apparently, 17 nm GNPs cause amnesia in mice, while 37 nm GNPs have no effect.

A dose–response curve for various concentrations of 17 nm GNPs was obtained. The passive-avoidance test was performed on mice injected with 17 nm GNPs at doses of 0, 0.4, 0.8, 1.9, 3.7, 7.3 and 14.6 mg kg^{-1}. The lowest concentration of GNPs with a significantly reduced latency time (138 ± 10 s) compared to the control group was 1.9 mg kg^{-1} ($p < 0.05$). The concentrations below 1.9 mg kg^{-1} had no significant effects. The latency time at higher doses was dose-dependent and plateaued rapidly at 7.3 mg kg^{-1}.

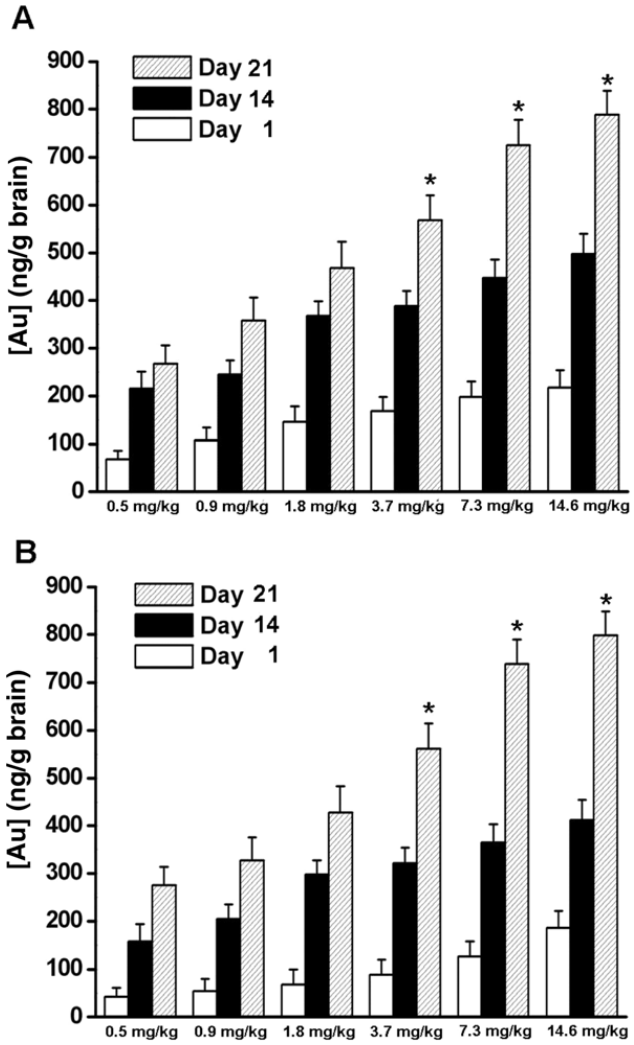

Figure 8. Accumulation of (A) 17 nm GNPs and (B) 37 nm GNPs in the brain. GNPs were injected intraperitoneally into mice at the indicated doses. Brain tissues were removed 1, 14 and 21 days after administering the GNPs. ICP-MS was performed to obtain the concentration of GNPs in brain tissue. Each value represents the average of six independent experiments and the error bars indicate standard deviation.

The monoamine and acetylcholine concentration profiles in the mouse brain were significantly affected by GNPs

Formation and consolidation of learning and memory are associated with the activity of acetylcholinergic, norepinephrinergic, dopaminergic and serotonergic neurons[33]. Most of these neurotransmitter systems can influence learning and memory in mice. GNP-treatment induced learning impairment, which indicated that GNPs might cause an imbalance of neurotransmitters in the mouse brain (figure 10). Norepinephrine negatively regulates the learning and memory process[34]. However, administration of scopolamine, 17 nm GNPs and 37 nm GNPs did not affect the levels of norepinephrine and its metabolite MHPG. Activation of the dopaminergic system also causes learning impairment[35-36]. GNP treatment elevated levels of dopamine from 114.5 ng g^{-1} brain to 143.6 ng g^{-1} brain for the 17 nm GNPs ($p < 0.01$), and to 138.2 for the 37 nm GNPs ($p < 0.05$). Serotonin was significantly reduced from 57.2 ng g^{-1} brain to 44.3 ng g^{-1} brain ($p < 0.05$) upon treatment with 17 nm GNPs[37]. Overall, GNPinduced learning impairment was correlated with an increase of dopamine and a decrease of serotonin in the mouse brain.

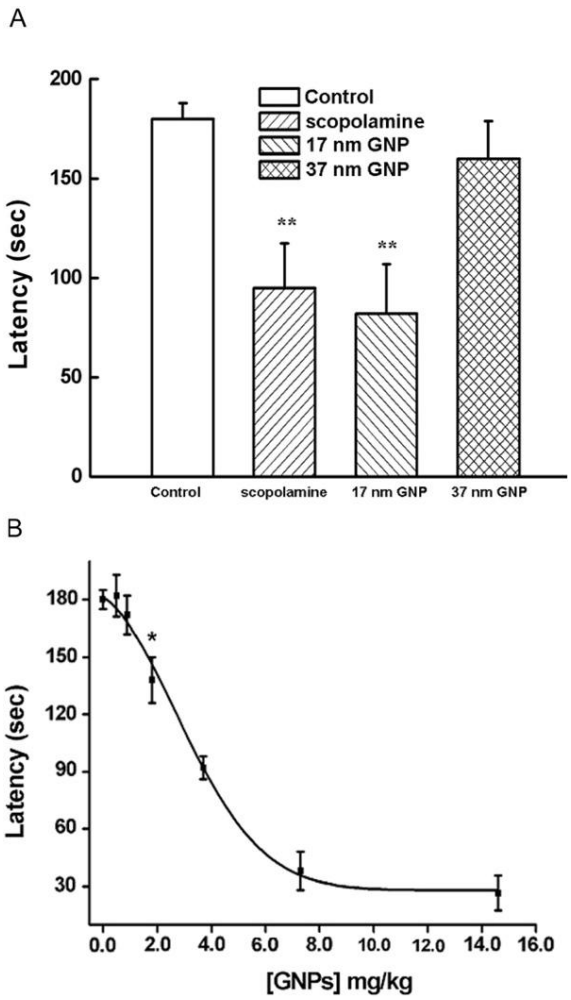

Figure 9. Learning impairment of passive-avoidance performance induced by scopolamine, 17 and 37 nm GNPs in mice. (A) Mice were randomly assigned to four groups, each containing 8–10 mice. The groups included a control group that did not receive any treatment, a positive control group that received scopolamine (1 mg kg^{-1} i.p.), the 17 nm GNP-treated group (3.7 mg kg^{-1}) and the 37 nm GNP-treated group (3.7 mg kg^{-1}). A passive-avoidance test was performed, and the averaged latency time is shown (** $p < 0.01$). (B) Dosage response of mice injected with 17 nm GNPs in the passive-avoidance test. The passive-avoidance test was performed on mice injected with 17 nm GNPs at doses of 0, 0.4, 0.8, 1.9, 3.7, 7.3 and 14.6 mg kg^{-1}. The latency of the control group was 180 s. The lowest concentration of GNPs with a significantly reduced latency time (138 s) compared to control group was 1.9 mg kg^{-1} (* $p < 0.05$). The concentrations below 1.9 mg kg^{-1} had no significant effects. The latency time at higher doses was dose-dependent and plateaued rapidly at 7.3 mg kg^{-1}.

The macroscopic distribution of 17 and 37 nm GNPs in the brain were indistinguishable

The differential effects of 17 and 37 nm GNPs on the cognition of mice implied that the distribution of GNPs in the brain might be size-dependent. ICP-MS was used to detect the distribution of GNPs in the mouse brain. After 21 days of GNP injection at a dose of 3.7 mg kg^{-1}, mouse brains were dissected into six parts: the left and right frontal lobes, left and right medial temporal lobes, and the left and right occipital lobes. Both 17 and 37 nm GNPs were detected in all parts of the brain at concentrations ranging from 496.2 to 559.5 ng g^{-1} brain. The lowest concentration was found in the occipital lobes (figure 11). We were unable to differentiate the macroscopic distributions of 17 and 37 nm GNPs in the samples. The ICP-MS results indicated that 17 and 37 nm GNPs were capable of passing through the blood–brain barrier and entering the mouse brain.

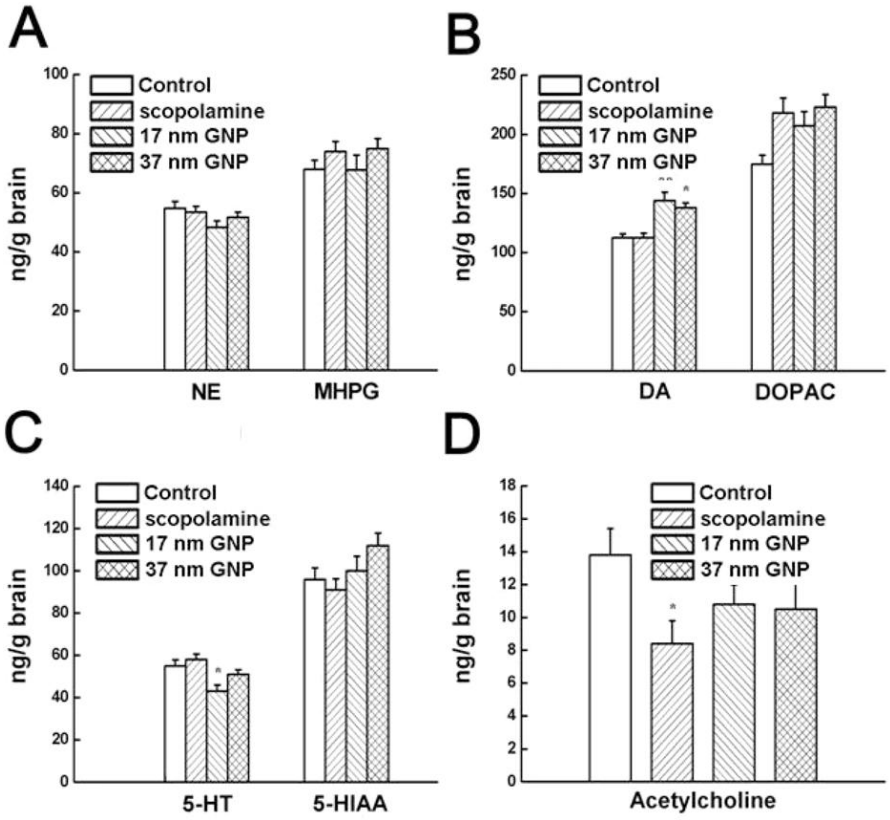

Figure 10. Fluctuation of monoamine and acetylcholine levels induced by scopolamine, 17 nm GNPs, and 37 nm GNPs in the mouse brain. Immediately after the passive-avoidance test, brain tissues were removed and levels of monoamines and acetylcholine were analyzed. The levels of neurotransmitters and their metabolites are shown in the plots. (A) Norepinephrine (NE) and 4-hydroxy-3-methoxyphenylglycol (MHPG). (B) Dopamine (DA) and 3,4-dihydroxyphenylacetic acid (DOPAC). (C) 5-hydroxytyramine (5-HT, serotonin) and 5-hydroxyindoleacetic acid (5-HIAA). (D) Acetylcholine. Each group of columns contains, in sequence, averaged values from the control group, the scopolamine-treated group, the 17 nm GNP-treated group and the 37 nm GNP-treated group. * indicates $p < 0.05$ and ** represents $p < 0.001$ from Student's t -test.

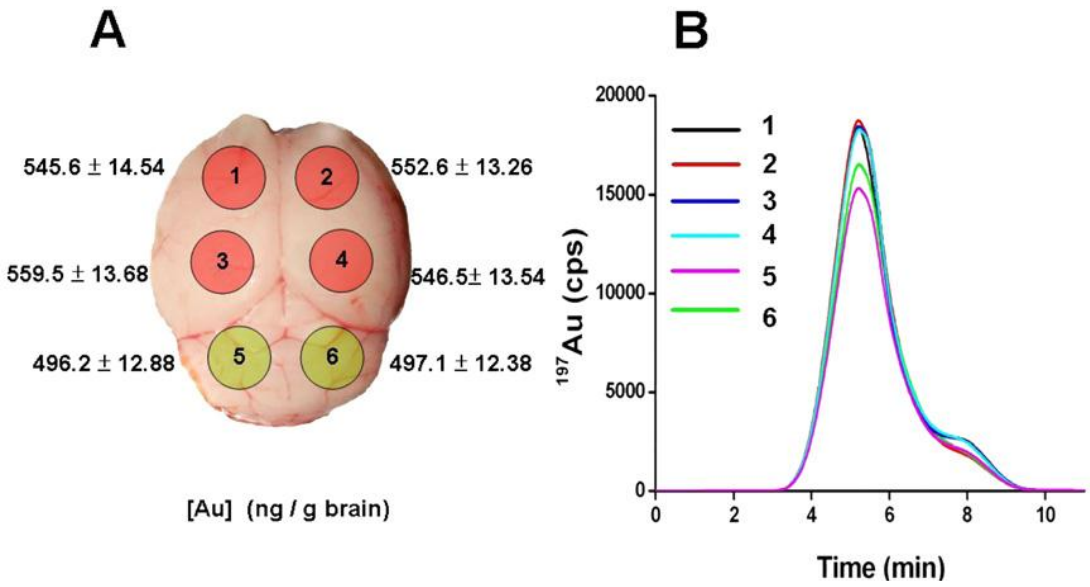

Figure 11. Global distribution of 17 nm GNPs in the mouse brain. (A) Schematic representation of the six areas dissected from the mouse brain and the corresponding 17 nm GNP concentrations based on the results of ICP-MS detection. These values represent the average of six independent experiments. (B) ICP-MS readings for typical samples were obtained from each part of the brain.

CARS microscopy differentiated the local distributions of 17 and 37 nm GNPs in the hippocampus

The hippocampus is located in the medial temporal lobe of the brain, belongs to the limbic system and plays major roles in short-term memory as well as spatial navigation. Since GNP injection impaired learning and memory in mice, the GNPs could have been transported through the blood, across the blood–brain barrier into the brain and into the hippocampus. To verify the presence of GNPs, the freshly dissected hippocampi were observed using *ex vivo* CARS microscopy (figure 12). GNPs are known to enhance the anti- Stokes Raman signal of nearby amino acids. With proper controls, the enhancement made possible by CARS strongly indicated the presence of GNPs. GNPs were also diffused *ex vivo* into brain tissues to verify the enhancement of Raman signal. Localized enhancement of an anti-Stokes Raman signal at an excitation wavelength of 817 nm was observed from the hippocampi removed from 17 and 37 nm GNP-treated mice. The Raman signal was completely absent from control mouse tissues. The Raman signal of 17 nm GNPs was localized to the Cornu Ammonis (CA) region of the hippocampus inside a cluster of neuronal cells, while 37 nm GNPs were scattered throughout the peripheral region. The distribution of 17 and 37 nm GNPs in the hippocampus suggested that the invasion of GNPs into the cluster of neuronal cells in the CA might have caused learning impairment in the 17 nm GNP-treated mice, while the 37 nm GNPs were incapable of entering neuronal cells and only caused minimal deficits in learning and memory.

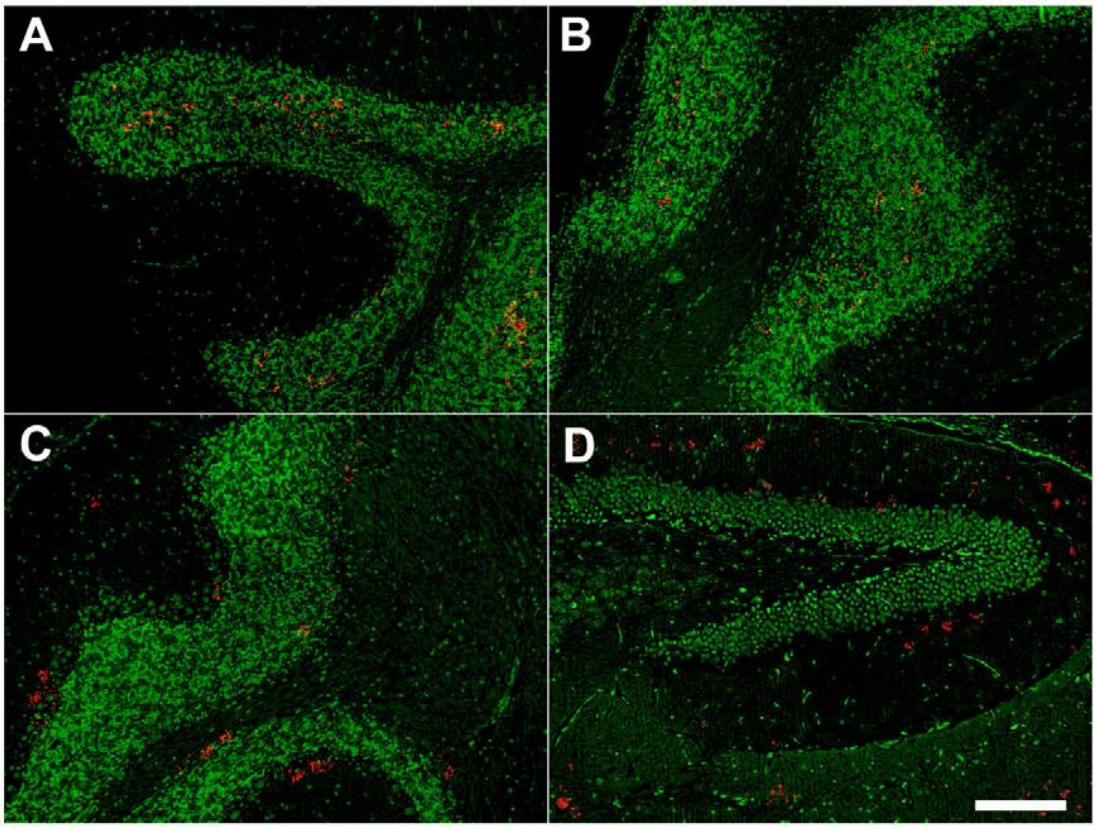

Figure 12. CARS microscopy of hippocampi isolated from 17 nm GNP-treated and 37 nm GNP-treated mice. The wavelengths of the pump and the Stokes lasers (Pump = 870 nm and Stokes = 1064 nm) were tuned to match a Raman shift (*2100 cm^{-1}) that fell in the so-called 'silent region' of the vibrational spectra of cells and tissues. To better visualize the location of GNPs, the enhanced bright spots are red in the final images. The green fluorescence is the auto-fluorescence emitted from the cells of the CA region in the hippocampus. (A), (B) Hippocampi obtained from 17 nm GNP-treated mice. (C), (D) Hippocampi obtained from 37 nm GNP-treated mice. Scalebar = 200 μm.

TEM revealed that 17 nm GNPs were located in the cytoplasm of hippocampal neurons while 37 nm GNPs were not

TEM was performed to verify the cytoplasmic location of the 17 and 37 nm GNPs in the hippocampus 21 days after the injection of GNPs (figures 13 and 14). A total of 72 TEM images were examined. We found that the 17 nm GNPs were located in the cytoplasm of pyramidal cells (figures 13(A)–(C)). The Au composition was verified using energy dispersive xray spectroscopy (EDS; figure 13(F)), and the gold was also detected using HR-TEM (figure 13(E)). The 17 nm GNPs were found to be associated with dendrites (figure 13(D)). In particular, the 17 nm GNPs were surrounded by coated pitlike structures in the cytoplasm, leading us to suspect that the 17 nm GNPs entered the cells through endocytosis. However, no endocytosis-related structures were found for the 17 nm GNPs at the dendrites. This result implies that these GNPs entered the dendrites through free diffusion. Additionally, these results suggest that alternative mechanisms for the cell uptake of GNPs occur together as previously reported. The invasion of metallic particles, such as GNPs, into neuronal cells and dendrites could seriously interfere with electric signals transmitted through the hippocampus, thereby inducing learning and memory impairments.

The presence of 37 nm GNPs in the hippocampus was also examined by TEM (figure 14). Several dark spots were noted in the cytoplasm of neuronal cells (figures 14(A)–(C)). Further examination with EDS revealed that these spots were composed of uranium, possibly due to the heterogeneity of the staining solution (figure 14(F)). Many 37 nm GNPs were detected inside the dendritic structure of brain cells. However, no endocytic structures were associated with 37 nm GNPs in the dendrites. Apparently, the 37 nm GNPs that entered dendrites through free diffusion were excluded from the cell bodies.

There, evidence overwhelming showed that GNPs have negligible toxicity in cultured cells. The *in vivo* biodistribution has been determined in mice and rats. However, no further evidence regarding the physiological impact in animals has been provided. In zebrafish, GNPs exhibited minimal *in vivo* toxicity with an embryo mortality less than 3%, while silver nanoparticles showed an almost 100% mortality. The difference in toxicity between gold and silver was due more to the unique chemistry of silver and less to a simple reduction in size. If the gold nanoparticles showed any size-dependent toxicity, this toxicity would be mild and the particles would be better tolerated than silver nanoparticles. For this reason, the delicate functions of the brain provided an opportunity to prove this hypothesis. These results showed that the injection of seemingly nontoxic GNPs can impair the learning and memory of mice at a sufficient dose. The reduction of cognitive ability was associated with the endocytosis of 17 nm GNPs into the neuronal cells in the CA region of the hippocampus. The observation that 37 nm GNPs were found in the extracellular region of the hippocampus was consistent with the inability of the GNPs to impair cognition in mice.

The differential effect of 17 and 37 nm GNPs on the cognition of mice indicated that physical diffusion could be a key process. The day 1 and day 14 dose–brain accumulation curves indicated that 17 nm GNPs crossed the blood–brain barrier faster than 37 nm GNPs (figure 8). The macroscopic biodistribution of the two GNPs within the brain were indistinguishable from one another. However, the monoamine and acetylcholine profiles were comparable. The microscopic evidence implied that 17 nm GNPs entered into the brain tissue and diffused faster than 37 nm GNPs. In CARS, the Raman signal of 17 nm GNPs was localized to the CA regions of the hippocampus inside the cluster of neuronal cells, while 37 nm GNPs were scattered through the

peripheral region. The distribution of 17 and 37 nm GNPs in the hippocampus implied that the invasion of GNPs into a cluster of neuronal cells in the CA might have caused learning impairment in the 17 nm GNP-treated mice. In contrast, 37 nm GNPs were unable to enter neuronal cells, and therefore caused only minimal deficits in learning and memory. The difference in the effects on cognition of the two GNPs was apparently caused by the difference in cell entry. Although both GNPs caused a global fluctuation in neurotransmitter levels in the brain, the differences in their invasive ability into the hippocampus determined the fate of the mice.

Binding of citrate at the gold surface was dynamic. It is possible that surface modifications that could have replaced citrate on the GNPs could have occurred after injection. Proteins such as albumin, immunoglobulins, complement, fibrinogen and apolipoproteins bind strongly to nanoparticles once the particles are in body fluids[38]. In particular, binding between complement and immunoglobulin (opsonization) promotes receptor-mediated phagocytosis[37,39]. Binding of plasma protein is important for determining the *in vivo* biodistribution of nanoparticles. This binding might explain how the injected GNPs passed through the blood–brain barrier and entered into the hippocampus.

The brain is the most delicate and complex organ in animals. Both GNPs in this study affected monoamine profiles in the brain, indicating that brain functions other than learning and memory might be affected by the injection of GNPs. The invading GNPs could also have caused the abnormal transmission of electrical signals through neurons. It is also possible that the engulfment of GNPs may induce an abnormal cellular response, such as apoptosis or an imbalance of intracellular electrolytes. Further experiments are necessary to explore the extent of the damaging effects of GNPs.

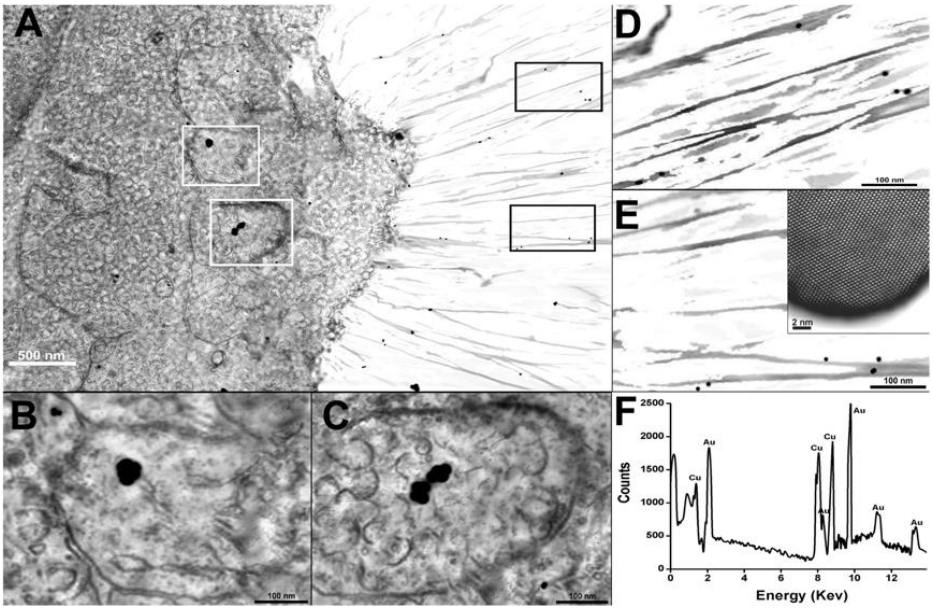

Figure 13. TEM images of neuronal cells from the hippocampus of a 17 nm GNP-treated mouse. (A) Entire view. (B), (C) Enlarged areas from (A) showing the invasion of 17 nm GNPs and the surrounding coated pit-like structures in the cytoplasm. (D) Enlarged area from (A) showing the association of GNPs with the dendrites. (E) is similar to (D) but contains an inset HR-TEM image showing the metallic nature of the black spots. (F) EDS of the selected GNPs in (B).

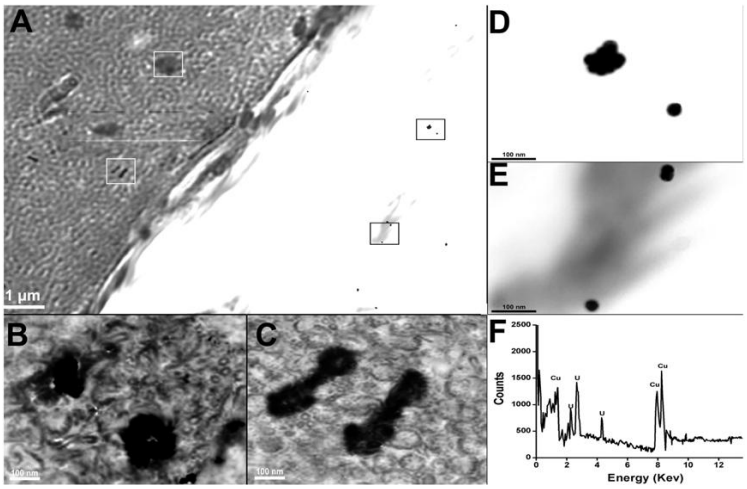

Figure 14. TEM images of neuronal cells from the hippocampus of a 37 nm GNP-treated mouse. (A) Entire view. (B), (C) Enlarged areas from (A) showing the dark spots. (D), (E) Enlarged areas from (A) showing the association of GNPs with dendrites. (F) EDS of the dark spots in (B) identifies these spots as uranium.

Preparation and analysis of pFMDV peptide and GNP conjugates

To further investigate the utility of GNPs as vaccine carriers, pFMDV was designed and synthesized based on its previously reported immunogenic epitope[19]. In particular, an extra cysteine residue was attached to the peptide's C-terminus to provide a sulfhydryl group as a conjugating site for the GNPs. The pFMDV was then conjugated to GNPs of various sizes (2, 5, 8, 12, 17, 37, and 50 nm in diameter). The synthesis of GNPs with varying diameters was monitored by UV absorbance (figure 15) and the resultant GNPs were examined by electron microscopy (figure 1). Conjugation of pFMDV–GNP was optimized by sodium chloride-induced aggregation[22]. More specifically, the lowest peptide concentration that did not cause a color change from red to dark blue, thus showing the lowest tendency to aggregate, was chosen for conjugation. The amount of pFMDV conjugated per GNP was also calculated as proportional to the surface area of the GNPs (figure16). Conjugation of peptide to GNPs was analyzed by gel electrophoresis, which indicated that stable pFMDV–GNP conjugates were generated (figure 17).

Induction of focused and enhanced antibody response by pFMDV–GNP conjugates

It has been shown that naked GNPs ranging from 8 to 17 nm in diameter are toxic to mice[25]. However, this toxicity is dose-dependent. In the current study, we administered GNPs at a dose of 0.5 mg kg^{-1}, which is one-sixteenth of the lethal dose and is apparently nontoxic to mice. Additionally, conjugation of pFMDV to the GNPs further reduced this *in vivo* toxicity, as the mice appeared healthy throughout the 10-week experimental period.

Mice were immunized with pFMDV–GNP conjugates that were prepared using GNPs of various sizes. Each injection contained equal amounts of pFMDV–GNP at a final concentration of 0.01 $\mu g\ \mu l^{-1}$. As a control, mice were injected with pFMDV–KLH at a final concentration of 0.01 mg ml^{-1}. These conjugates were injected IP and SC into BALB/c mice weekly, starting at week 0. Tail blood was collected after 4, 6, 8, and 10 weeks, followed by ELISA analysis to obtain titers of antisera against pFMDV, GNPs, and KLH (figures 5 and 6).

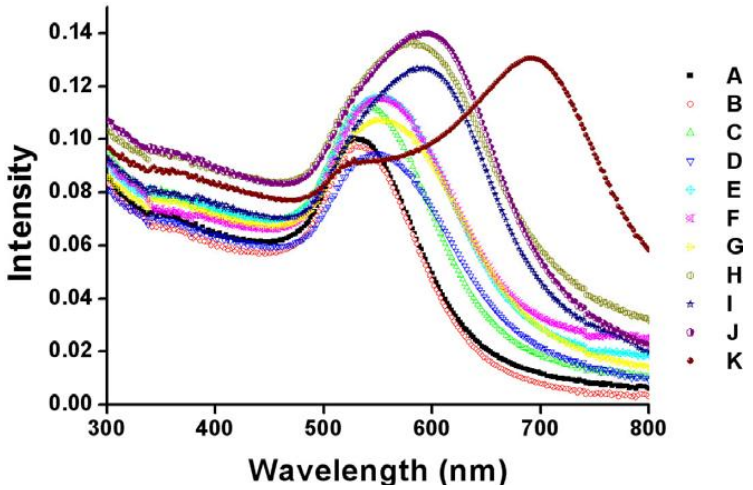

Figure 15. UV–vis absorbance measurements of GNPs. A shift of the surface plasmon band peaks correlated with different concentrations of peptides. Concentrations of pFMDV were: A, 1 μM; B, 0.9 μM; C, 0.8 μM; D, 0.7 μM; E, 06 μM; F, 0.5 μM; G, 0.4 μM; H, 0.3 μM; I, 0.2 μM; J, 0.1 μM; and K, 0 μM.

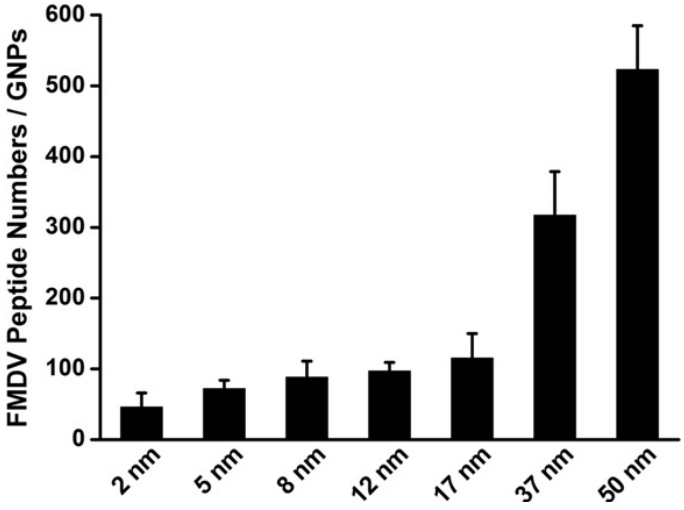

Figure 16. Number of pFMDVs conjugated to GNPs versus GNP diameter. The amount of conjugated pFMDV on the surface of the GNPs was calculated from the saturating concentration of the titration curves. The amount of conjugated pFMDV was proportional to the surface area of the GNPs.

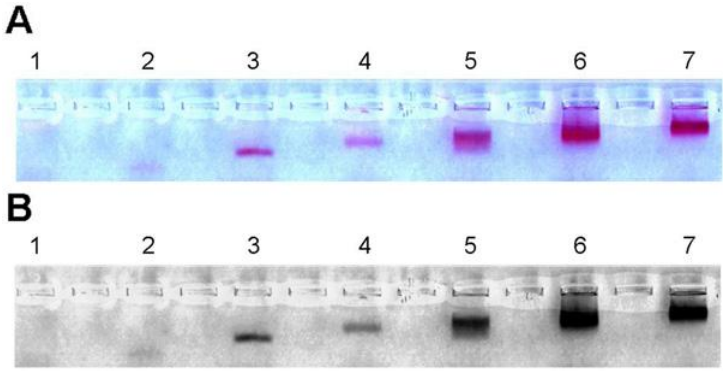

Figure 17. Gel electrophoresis of pFMDV–GNP conjugates. (A) Electrophoresis performed without staining. (B) Gel staining with Coomassie Brilliant Blue to indicate the presence of pFMDV. The difference in protein mobility was attributed to differences in the size of GNPs adsorbed to the pFMDVs. pFMDV–GNP conjugates were loaded as follows: lane 1, 2 nm GNPs; lane 2, 5 nm GNPs; lane 3, 8 nm GNPs; lane 4, 12 nm GNPs; lane 5, 17 nm GNPs; lane 6, 37 nm GNPs; and lane 7, 50 nm GNPs.

A significant antibody response was noted at week 6 (figure 18). The binding affinity of the antibodies, using pFMDV as the antigen, indicated size dependency. The pFMDV–2 nm GNP induced a titer of 19 000 ± 1900 at week 6, and this titer increased when GNP size was augmented. Antibody levels peaked when 8 nm diameter GNPs were administered (62 000 ± 3100) and then decreased to 0 for 37 and 50 nm GNPs at week 6. Meanwhile, the pFMDV–KLH conjugate exhibited a medium-strength antibody response, with a titer of 20 000 ± 1700. A three-fold enhancement of the antibody titers was observed using the GNPs as a carrier,as compared to using KLH.

When antibody responses at weeks 4, 6, 8, and 10 were integrated, a clear size-dependent relationship between GNPs and antibody levels was observed (figure 19(A)). GNPs ranging from 2 to 8 nm in diameter exhibited increasing binding affinity following subsequent immunizations, with the highest affinity associated with 8 nm GNPs. Meanwhile, a gradual decrease in the antibody titer was observed for the 12 and 17 nm diameter GNPs over time. We could not observe induced binding activity for the conjugates prepared with 37 and 50 nm diameter GNPs until the end of the experiment. In contrast to the GNP conjugates, the KLH conjugate exhibited medium-strength binding affinity.

The antibody response to carriers plays an important role in determining the immunogenicity of the conjugated peptide. While an ideal carrier should remain silent during immunization with peptide, KLH and other carriers are known to induce a significant immune response[23-24,40]. Antisera against KLH were observed beginning at week 4 and increased to a significant level (110 000 ± 6700) by week 10 (figure 19(B)). In contrast, GNPs, regardless of their size, showed no detectable antibody-binding activity over the course of our experiment. Thus, GNPs were demonstrated to be ideal candidate vaccine carriers due to their lack of immunogenicity.

In sum, we demonstrated that GNPs can act as vaccine carriers, inducing an approximately three-fold enhancement in immunogenicity, as compared to responses elicited by the control vaccine carrier. Furthermore, the GNPs induced no detectable antibody binding when the two were incubated together. The GNPs used in this study thus possessed all of the positive characteristics of an ideal vaccine carrier.

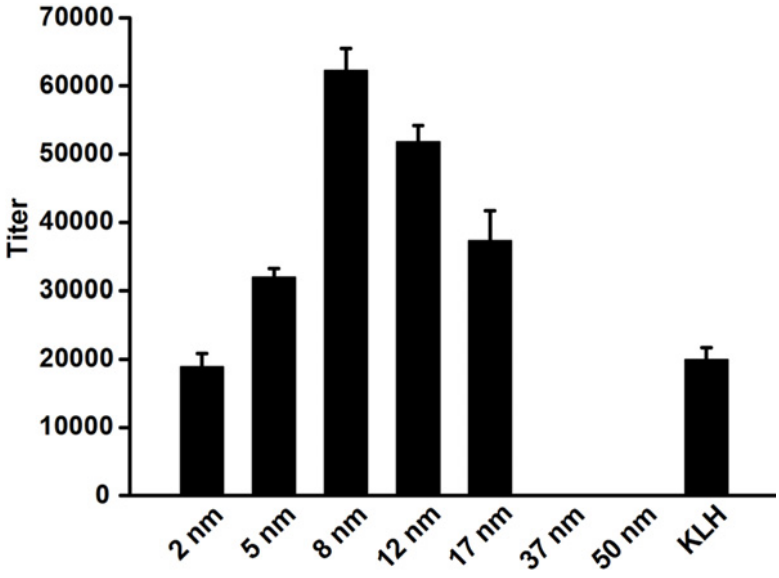

Figure 18. Titers of antisera withdrawn from pFMDV–GNP-injected mice on the sixth week of immunization. The values are averaged from samples derived from six different mice. The titer resulting from pFMDV–KLH immunization served as a control. Sera obtained from pFMDV–37 nm GNP- and pFMDV–50 nm GNP-injected mice did not exhibit detectable binding activity.

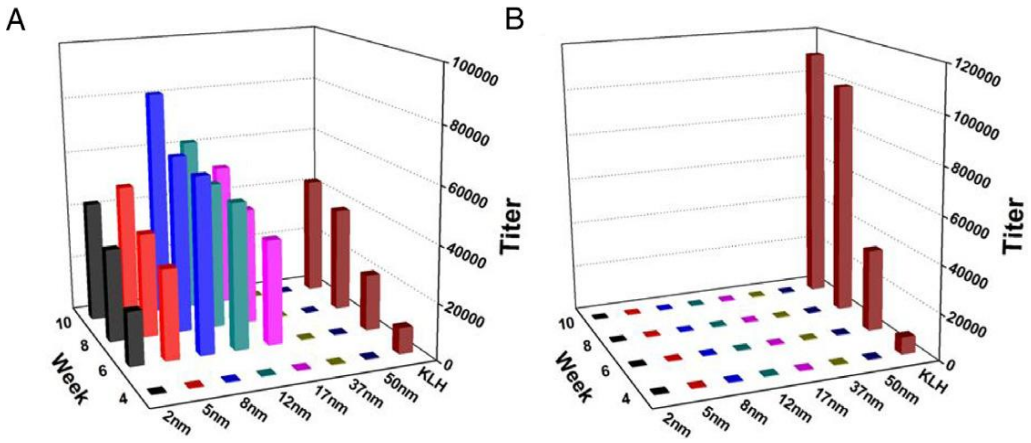

Figure 19. Titers of antisera from pFMDV–GNP-injected mice on weeks 4, 6, 8, and 10. The antigens used in the ELISA were (A) pFMDV and (B) GNPs/KLH. Titers of pFMDV–KLH were incorporated as a control.

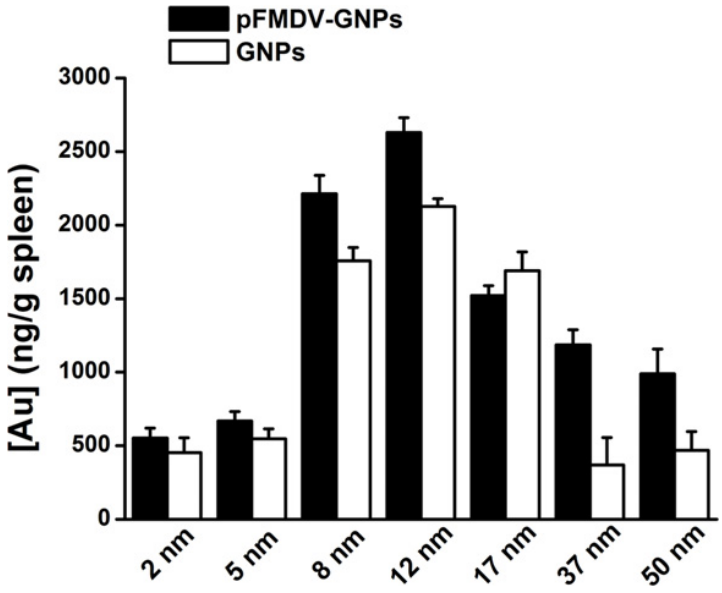

Figure 20. Distribution of GNPs in the mouse spleen. The pFMDV–GNP-injected mice were sacrificed at the end of the experiment. Numbers of GNPs in the spleen were then quantified by ICP-MS. Mice injected with pFMDV–GNPs are represented by the filled columns. The biodistribution of unmodified GNPs is represented by the empty columns. The values are averaged from six mice.

Antibody response elicited by pFMDV–GNP conjugates associated with the number of GNPs taken up by spleen

The pFMDV–GNP conjugates may be taken up by antigenpresenting cells (APCs), including macrophages and dendritic cells. Typically, these APCs are transported by the circulation to the spleen. Epitopes presented on the surface of APCs are recognized by T cells, leading to subsequent T-cell activation. The presence and accumulation of pFMDV–GNPs in the spleen ensures the effective induction of an immune response toward the peptide.

The number of pFMDV–GNPs in the spleen was evaluated by ICP-MS (figure 20). The pFMDV–GNPs showed sizedependent biodistribution in the spleen. Indeed, their distribution profile in the spleen showed a

striking similarity to their antibody-binding profile (figure 19), with maximal accumulation for the 12 nm GNPs.

The ability of GNPs to carry conjugated peptides into the spleen seemed to depend solely on the diameter of the GNP. When naked GNPs were injected into mice, their biodistribution in the spleen was almost identical to that of pFMDV–GNP conjugates (figure 20). This similarity indicated that surface modification of the GNPs did not alter their ability to enter the spleen. The similar biodistribution of naked and peptide-conjugated GNPs also demonstrated the size-dependent ability of GNPs to invade and accumulate in the spleen.

TEM was performed to verify the presence of GNPs in the spleen (figure 21) and showed that particles from 2 to 50 nm in diameter were trapped in splenic vesicles. The number of vesicular GNPs was minimal at diameters of 2 and 5 nm, maximal for diameters of 8 and 12 nm, and intermediate for 17–50 nm GNPs. These TEM results are consistent with the distribution profile obtained by ICP-MS.

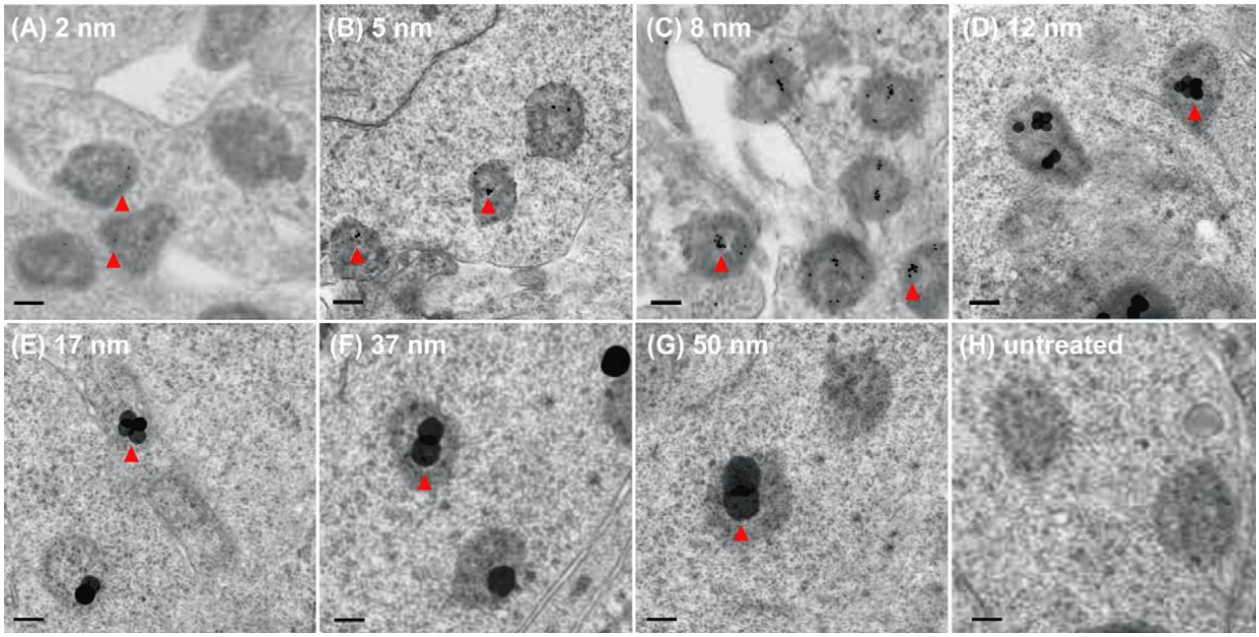

Figure 21. TEM images of spleens obtained from pFMDV–GNP-immunized mice. Mice were injected with pFMDV–GNPs of various GNP diameters: (A) 2 nm GNP, (B) 5 nm GNP, (C) 8 nm GNP, (D) 12 nm GNP, (E) 17 nm GNP, (F) 37 nm GNP, and (G) 50 nm GNP. The arrows indicate the aggregation and accumulation of GNPs in the vesicles of the spleen cells (scale bars are 20 nm).

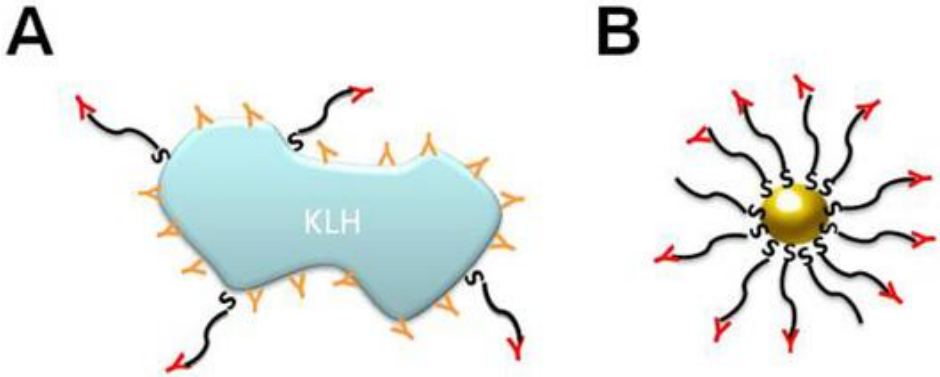

Figure 22. Schematic representation of the focused immunogenicity of KLH and GNPs as vaccine carriers. (A) Antibodies generated against peptide–KLH conjugates recognize epitopes displayed on both the peptide and KLH. (B) Antibodies generated by peptide–GNP conjugates selectively recognize peptide epitopes and rarely bind to the GNPs.

A focused antibody response against haptens has several benefits. One application of such a strong response is more effective, less tedious production of monoclonal antibodies. This antiserum may also be used in assays that require highly specific antibody–antigen interactions, such as western blots. The benefits of the low response towards the gold particles are not only economic but also time-saving.

It was reported that peptide–KLH conjugates induce a strong immune response in mice. Additionally, KLH exhibits non-specific binding to the antigen and gives rise to falsepositive binding due to this cross-reactivity. In this study, KLH induced a strong immune response against itself, with an antibody titer that was higher than that raised against pFMDV alone (figure 19). It is likely that conjugation of pFMDV to KLH generated potent antibody-recognition sites, thus complicating the induced antibody specificity. Antisera strongly recognized both the pFMDV–KLH conjugates and KLH alone, so specific binding to the synthetic pFMDV was seriously reduced (figure 22(A)).

In contrast to KLH carriers, the humoral response to GNPs is undetectable. However, when the GNPs were conjugated to pFMDV, they induced a strong antibody response specific to pFMDV, but rarely to the particles themselves (figure 22(B)). The finding indicates that the antibody response to synthetic pFMDV was not altered by conjugation to GNPs. GNPs are thus inert, rendering them ideal candidate vaccine carriers.

It is possible that the immune response induced by pFMDV is proportional to the number of peptides conjugated to the GNPs. However, this is unlikely because the total amount of peptide per injection remained constant. Furthermore, as determined by a titration test (figure 15) and gel electrophoresis (figure 17), the number of peptides per GNP was proportional to the particle's surface area (figure 16) but was not correlated with the size-dependent antibody response profile.

In rare cases, naked GNPs may induce antibody responses that affect the immunogenicity and specificity of peptide–GNP conjugates. In a previous study[25], we demonstrated that sera obtained from mice injected with GNPs that were 5 nm in diameter or smaller showed antibody-binding activity against the corresponding GNPs. However, the GNP-specific antibody titer was approximately 1000, which is at the lower boundary of titer values classified as positive binding. Adjuvant administration did not enhance the production of GNP-specific antisera, indicated by unchanged antibody binding to the GNPs. Therefore, the immunogenic binding activity of GNPs smaller than 5 nm in diameter is insignificant compared to the antibody response generated against the conjugated synthetic peptide.

The number of GNPs that accumulated in the spleen was size-dependent, as evaluated by ICP-MS (figure 20) and TEM (figure 21). The accumulation profile matched the sizedependent pattern of the immune response. This result is consistent with that of a previous nanovaccine study using 25 and 100 nm diameter pluronic-stabilized PPS nanoparticles as vaccine carriers[41]. This study demonstrated that generation of humoral and cellular immunity in mice is size- and complement-dependent. After intradermal injection, 25 nm nanoparticles were efficiently transported into the lymphatic capillaries and their draining lymph nodes, whereas 100 nm nanoparticles were only 10% as efficiently transported. Further studies should provide insights into the size-dependent immunogenicity of GNPs.

The potential benefits of using GNPs instead of traditional vaccine carriers are their low immunogenicity and ability to enhance the immune response to the conjugated peptide. Although this combination is seemingly contradictory, it may be realized by the size-dependent GNP biodistribution in the spleen, as observed by ICP-MS. It has been reported that endocytosis is dependent on the size and shape of

GNPs[10-11]. In this study, GNP endocytosis reached a maximum when GNP diameter approached 50 nm. Additionally, larger GNPs tended to accumulate in the cells rather than in the circulation. It is possible that the majority of injected GNPs were absorbed at the site of injection[42] and that the slow release of larger particles resulted in a reduced number of larger particles in the blood. Consistent with this hypothesis, the majority of GNPs found in the circulation were 8–12 nm in diameter[28,43]. Therefore, the accumulation of larger GNPs in the spleen could be due to size-dependent differences in GNP plasma concentration. The enhancement of the immune response by GNP carrier may thus be the consequence of increased localization to the spleen.

In the control group, unmodified GNPs also exhibited the same size-dependent biodistribution and the number of pFMDV–GNP conjugates in the spleen was higher than that of unmodified GNPs. These results indicate that peptide modification enhances both construct uptake by APCs and construct accumulation in the spleen.

Thus, we showed that the size-dependent immunogenicity of the pFMDV–GNP conjugates was associated with the number of GNPs taken up by the spleen. GNPs ranging from 8 to 17 nm in diameter may thus serve as ideal vaccine carriers,eliciting focused antibody responses against synthetic peptides.

Conclusions

The environmental impact of nanoparticles is evident; however, their toxicity due to their nanosize is rarely discussed. Gold nanoparticles (GNPs) may serve as a promising model to address the size-dependent biological response to nanoparticles because they show good biocompatibility and their size can be controlled with great precision during their chemical synthesis.

We have shown heavy-dosed and naked GNPs are lethal to mice. Mice injected with GNPs ranging from 8 nm to 37 nm showed fatigue, loss of appetite, change of fur color, and weight loss. The majority of mice in these groups died within 21 days. Injection of 5 nm and 3 nm GNPs, or GNPs larger than 50 nm, however, did not induce sickness or lethality in mice. The toxicity of GNPs is size-dependent and closely associated with the ability to induce antibody response.

GNPs serve as an ideal vaccine carrier. We demonstrate the size-dependent immunogenic properties of pFMDV-GNP conjugates. GNPs ranging from 8 nm to 17 nm in diameter may be ideal for eliciting a focused antibody response against a synthetic pFMDV peptide.

GNPs impair cognition in mice. GNPs affected dopaminergic and serotonergic neurons. The ability of GNPs to damage cognition in mice is size-dependent and associated with the ability of the particles to invade the hippocampus. The dosage and duration of the treatment should be taken into account if GNPs are used in the future as vehicles to carry therapeutic agents into the brain.

Reference

1 Borm, P. J. & Muller-Schulte, D. Nanoparticles in drug delivery and environmental exposure: same size, same risks? *Nanomedicine (Lond)* **1**, 235-249, doi:10.2217/17435889.1.2.235 (2006).

2 Borm, P. J. *et al.* The potential risks of nanomaterials: a review carried out for ECETOC. *Part Fibre Toxicol* **3**, 11, doi:1743-8977-3-11 [pii] 10.1186/1743-8977-3-11 (2006).

3 Guzman, K. A., Taylor, M. R. & Banfield, J. F. Environmental risks of nanotechnology: National Nanotechnology Initiative funding, 2000-2004. *Environ Sci Technol* **40**, 1401-1407 (2006).

4 Carrero-Sanchez, J. C. *et al.* Biocompatibility and toxicological studies of carbon nanotubes doped with nitrogen. *Nano Lett* **6**, 1609-1616, doi:10.1021/nl060548p (2006).

5 Fiorito, S., Serafino, A., Andreola, F., Togna, A. & Togna, G. Toxicity and biocompatibility of carbon nanoparticles. *J Nanosci Nanotechnol* **6**, 591-599 (2006).

6 Zhu, S., Oberdorster, E. & Haasch, M. L. Toxicity of an engineered nanoparticle (fullerene, C60) in two aquatic species, Daphnia and fathead minnow. *Mar Environ Res* **62 Suppl**, S5-9, doi:S0141-1136(06)00044-4 [pii] 10.1016/j.marenvres.2006.04.059 (2006).

7 Federici, G., Shaw, B. J. & Handy, R. D. Toxicity of titanium dioxide nanoparticles to rainbow trout (Oncorhynchus mykiss): gill injury, oxidative stress, and other physiological effects. *Aquat Toxicol* **84**, 415-430, doi:S0166-445X(07)00272-X [pii] 10.1016/j.aquatox.2007.07.009 (2007).

8 Park, J., Bauer, S., von der Mark, K. & Schmuki, P. Nanosize and vitality: TiO2 nanotube diameter directs cell fate. *Nano Lett* **7**, 1686-1691, doi:10.1021/nl070678d (2007).

9 Gurr, J. R., Wang, A. S., Chen, C. H. & Jan, K. Y. Ultrafine titanium dioxide particles in the absence of photoactivation can induce oxidative damage to human bronchial epithelial cells. *Toxicology* **213**, 66-73, doi:S0300-483X(05)00227-1 [pii] 10.1016/j.tox.2005.05.007 (2005).

10 Chithrani, B. D., Ghazani, A. A. & Chan, W. C. Determining the size and shape dependence of gold nanoparticle uptake into mammalian cells. *Nano Lett* **6**, 662-668, doi:10.1021/nl052396o (2006).

11 Chithrani, B. D. & Chan, W. C. Elucidating the mechanism of cellular uptake and removal of protein-coated gold nanoparticles of different sizes and shapes. *Nano Lett* **7**, 1542-1550, doi:10.1021/nl070363y (2007).

12 Becker, M. L., Bailey, L. O. & Wooley, K. L. Peptide-derivatized shell-cross-linked nanoparticles. 2. Biocompatibility evaluation. *Bioconjug Chem* **15**, 710-717, doi:10.1021/bc049945m (2004).

13 Connor, E. E., Mwamuka, J., Gole, A., Murphy, C. J. & Wyatt, M. D. Gold nanoparticles are taken up by human cells but do not cause acute cytotoxicity. *Small* **1**, 325-327, doi:10.1002/smll.200400093 (2005).

14 Hauck, T. S. & Chan, W. C. Gold nanoshells in cancer imaging and therapy: towards clinical application. *Nanomedicine (Lond)* **2**, 735-738, doi:10.2217/17435889.2.5.735 (2007).

15 Paciotti, G. F. *et al.* Colloidal gold: a novel nanoparticle vector for tumor directed drug delivery. *Drug Deliv* **11**, 169-183, doi:10.1080/10717540490433895 2PLY5CG1FR8GVUVF [pii] (2004).

16 Brown, K. R., Walter, D. G. & Natan, M. J. Seeding of colloidal Au nanoparticle solutions. 2. Improved control of particle size and shape. *Chem Mater* **12**, 306-313 (2000).

17 Liu, F. K. *et al.* Microwave heating for the preparation of nanometer gold particles. *Jpn J Appl Phys 1*

42, 4152-4158, doi:Doi 10.1143/Jjap.42.4152 (2003).

18 Hsieh, M. T., Wu, C. R. & Hsieh, C. C. Ameliorating effect of p-hydroxybenzyl alcohol on cycloheximide-induced impairment of passive avoidance response in rats: interactions with compounds acting at 5-HT1A and 5-HT2 receptors. *Pharmacol Biochem Behav* **60**, 337-343, doi:S0091-3057(97)00591-1 [pii] (1998).

19 Shieh, J. J. *et al.* Enhancement of the immunity to foot-and-mouth disease virus by DNA priming and protein boosting immunization. *Vaccine* **19**, 4002-4010 (2001).

20 Brown, K. R., Ricci, F. M. & Ottesen, E. A. Ivermectin: effectiveness in lymphatic filariasis. *Parasitology* **121 Suppl**, S133-146 (2000).

21 Engvall, E. & Perlmann, P. Enzyme-linked immunosorbent assay (ELISA). Quantitative assay of immunoglobulin G. *Immunochemistry* **8**, 871-874 (1971).

22 Jacobs, I., Schele, R. & Sjodin, B. Blood lactate vs. exhaustive exercise to evaluate aerobic fitness. *Eur J Appl Physiol Occup Physiol* **54**, 151-155 (1985).

23 Beekman, N. J. C. M., Schaaper, W. M. M., Turkstra, J. A. & Meloen, R. H. Highly immunogenic and fully synthetic peptide-carrier constructs targetting GnRH. *Vaccine* **17**, 2043-2050 (1999).

24 Gharavi, A. E. *et al.* GDKV-induced antiphospholipid antibodies enhance thrombosis and activate endothelial cells in vivo and in vitro. *Journal of Immunology* **163**, 2922-2927 (1999).

25 Chen, Y. S., Hung, Y. C., Liau, I. & Huang, G. S. Assessment of the In Vivo Toxicity of Gold Nanoparticles. *Nanoscale Res Lett* **4**, 858-864, doi:DOI 10.1007/s11671-009-9334-6 (2009).

26 Sadauskas, E. *et al.* Kupffer cells are central in the removal of nanoparticles from the organism. *Part Fibre Toxicol* **4**, 10, doi:1743-8977-4-10 [pii] 10.1186/1743-8977-4-10 (2007).

27 Evans, C. L. *et al.* Chemical imaging of tissue in vivo with video-rate coherent anti-Stokes Raman scattering microscopy. *Proc. Natl. Acad. Sci. U. S. A.* **102**, 16807-16812, doi:DOI 10.1073/pnas.0508282102 (2005).

28 Sonavane, G., Tomoda, K. & Makino, K. Biodistribution of colloidal gold nanoparticles after intravenous administration: effect of particle size. *Colloids Surf B Biointerfaces* **66**, 274-280, doi:S0927-7765(08)00269-5 [pii] 10.1016/j.colsurfb.2008.07.004 (2008).

29 Patra, C. R. *et al.* Targeted delivery of gemcitabine to pancreatic adenocarcinoma using cetuximab as a targeting agent. *Cancer Res* **68**, 1970-1978, doi:68/6/1970 [pii] 10.1158/0008-5472.CAN-07-6102 (2008).

30 Rothen-Rutishauser, B. M., Schurch, S., Haenni, B., Kapp, N. & Gehr, P. Interaction of fine particles and nanoparticles with red blood cells visualized with advanced microscopic techniques. *Environ Sci Technol* **40**, 4353-4359 (2006).

31 Huang, G. S., Chen, Y. S. & Yeh, H. W. Measuring the flexibility of immunoglobulin by gold nanoparticles. *Nano Lett* **6**, 2467-2471, doi:10.1021/nl061598x (2006).

32 Choi, H. S. *et al.* Renal clearance of quantum dots. *Nat Biotechnol* **25**, 1165-1170, doi:nbt1340 [pii] 10.1038/nbt1340 (2007).

33 Myhrer, T. Neurotransmitter systems involved in learning and memory in the rat: a meta-analysis based on studies of four behavioral tasks. *Brain Res Rev* **41**, 268-287, doi:Doi 10.1016/S0165-0173(02)00268-0 (2003).

34 Thomas, S. A. & Palmiter, R. D. Disruption of the dopamine beta-hydroxylase gene in mice suggests roles for norepinephrine in motor function, learning, and memory. *Behav Neurosci* **111**, 579-589 (1997).

35 Denenberg, V. H., Kim, D. S. & Palmiter, R. D. The role of dopamine in learning, memory, and performance of a water escape task. *Behavioural Brain Research* **148**, 73-78, doi:Doi 10.1016/S0166-4328(03)00183-9 (2004).

36 Spanagel, R. & Weiss, F. The dopamine hypothesis of reward: past and current status. *Trends Neurosci* **22**, 521-527 (1999).

37 Owens, D. E., 3rd & Peppas, N. A. Opsonization, biodistribution, and pharmacokinetics of polymeric nanoparticles. *Int J Pharm* **307**, 93-102, doi:S0378-5173(05)00668-X [pii] 10.1016/j.ijpharm.2005.10.010 (2006).

38 Nel, A. E. *et al.* Understanding biophysicochemical interactions at the nano-bio interface. *Nat Mater* **8**, 543-557, doi:nmat2442 [pii] 10.1038/nmat2442 (2009).

39 Dobrovolskaia, M. A. & McNeil, S. E. Immunological properties of engineered nanomaterials. *Nat Nanotechnol* **2**, 469-478, doi:nnano.2007.223 [pii] 10.1038/nnano.2007.223 (2007).

40 May, R. J., Beenhouwer, D. O. & Scharff, M. D. Antibodies to keyhole limpet hemocyanin cross-react with an epitope on the polysaccharide capsule of Cryptococcus neoformans and other carbohydrates: Implications for vaccine development. *Journal of Immunology* **171**, 4905-4912 (2003).

41 Reddy, S. T. *et al.* Exploiting lymphatic transport and complement activation in nanoparticle vaccines. *Nat Biotechnol* **25**, 1159-1164, doi:nbt1332 [pii] 10.1038/nbt1332 (2007).

42 Manolova, V. *et al.* Nanoparticles target distinct dendritic cell populations according to their size. *Eur J Immunol* **38**, 1404-1413, doi:10.1002/eji.200737984 (2008).

43 Hauck, T. S., Ghazani, A. A. & Chan, W. C. Assessing the effect of surface chemistry on gold nanorod uptake, toxicity, and gene expression in mammalian cells. *Small* **4**, 153-159, doi:10.1002/smll.200700217 (2008).

國科會補助專題研究計畫成果報告自評表

請就研究內容與原計畫相符程度、達成預期目標情況、研究成果之學術或應用價值（簡要敘述成果所代表之意義、價值、影響或進一步發展之可能性）、是否適合在學術期刊發表或申請專利、主要發現或其他有關價值等，作一綜合評估。

1. 請就研究內容與原計畫相符程度、達成預期目標情況作一綜合評估

■ 達成目標

□ 未達成目標（請說明，以 100 字為限）

□ 實驗失敗

□ 因故實驗中斷

□ 其他原因

說明：

2. 研究成果在學術期刊發表或申請專利等情形：

論文：■已發表 □未發表之文稿 □撰寫中 □無

專利：□已獲得 □申請中 ■無

技轉：□已技轉 □洽談中 ■無

其他：（以 100 字為限）

3. 請依學術成就、技術創新、社會影響等方面，評估研究成果之學術或應用價值（簡要敘述成果所代表之意義、價值、影響或進一步發展之可能性）（以 500 字為限）

a. 評估奈米粒子對環境、生物體造成毒性的影響

b. 發展奈米金粒子作為疫苗製作的載體

c. 評估奈米金粒子做為藥物載體時較佳的施用濃度及施用時間